8-27-2012

Numerical analysis of plastic deformation in metal-ceramic nanolayers during cyclic indentation

Caroline Bolton Blada

Caroline Bolton Blada
Candidate

Mechacnical Engineering
Department

This thesis is approved, and it is acceptable in quality and form for publication:

Approved by the Thesis Committee:

Yu-Lin Shen , Chairperson

Tariq Khraishi

Zayd Leseman

Numerical Analysis of Plastic Deformation in Metal-Ceramic Nanolayers During Cyclic Indentation

by

Caroline Bolton Blada

B.S., Mechanical Engineering, University of New Mexico, 2010

THESIS

Submitted in Partial Fulfillment of the
Requirements for the Degree of

Master of Science
Mechanical Engineering

The University of New Mexico

Albuquerque, New Mexico

June, 2012

Dedication

To my husband and my family for their continued support.

Acknowledgments

It would not have been possible to write this thesis without the help and support of the kind people around me.

I would like to express my deep and sincere gratitude to my advisor, Dr. Yu-Lin Shen, whose patience and kindness, as well as his academic experience, have been invaluable to me. I am thankful for his encouragement and guidance.

I would like to thank Dr. Tariq Khraishi and Dr. Zayd Leseman for serving on my thesis committee and providing their professional expertise.

Finally, I would like to thank all of my friends and family for their invaluable support.

Numerical Analysis of Plastic Deformation in Metal-Ceramic Nanolayers During Cyclic Indentation

by

Caroline Bolton Blada

B.S., Mechanical Engineering, University of New Mexico, 2010

M.S., Mechanical Engineering, University of New Mexico, 2012

Abstract

The indentation behavior of metal/ceramic nanolayered composites is studied numerically using the finite element method. Attention is devoted to cyclic response under fixed maximum and minimum loads, with the primary objective of examining the evolving plastic deformation in the ductile metal constrained by the hard ceramic layers. An axisymmetric model consisting of alternating aluminum (Al) and silicon carbide (SiC) thin films on a silicon (Si) substrate is indented by a conical diamond indenter. In this study, both rate-independent and rate-dependent plasticity models are considered. It is found that, in the multilayered material plastic deformation in the Al layers continues to occur upon unloading and subsequent loading /unloading operations. The cyclic plasticity results in an open load-displacement loop, and the indenter continues to move deeper with each cycle. For the control model of a homogeneous Al film, there is no hysteresis loop and transient behavior soon approaches stabilization, showing repetitive elastic loading/unloading. The modeling results are also compared with cyclic nanoindentation experiments conducted on the same

metal-ceramic multilayer system and control specimen. The modeling results are in qualitative agreement with the actual cyclic nanoindentation experiment conducted on the Al/SiC nanolayers.

Contents

List of Figures

List of Tables

Chapter 1

Introduction

Finite element modeling (FEM) has become one of the most prevalent techniques used to analyze and examine the reaction of solid materials to internal and external forces [1–8]. Indentation (micro- and nano-) is an especially attractive test to model because not only does it save time, but the testing parameters and material properties can be easily changed. The knowledge of the material constitutive laws is important for the prediction of material behavior. The mechanical properties of materials can be investigated by means of computational experimental procedures. Indentation tests can be used to evaluate the strength of materials and coatings. These tests are based on the relationship between the applied indenter load per contact area and the plastic flow strength of the material.

Relevant properties of thin films can be determined by indentation tests. Nanoindentation is the technique most commonly used to characterize the properties of thin films [9, 10]. The results of nanoindentation are greatly affected by many factors; indentation depth, substrate properties, specimen geometry, etc. Indentation is a severe form of deformation, leading to large strains and issues where materials behave nonlinearly. FEM of nanoindentation is useful to explore how different factors

affect modeling results, as well as obtaining unknown data that cannot be collected experimentally. Nanoindentation tests continuously register the applied force of the indenter as well as indenter depth. Using the FEM method, quantitative stress and strain information can be used to estimate certain properties of the film, such as elastic modulus, hardness and fracture toughness.

Thin films can be used for a variety of reasons, one of the most common being coating on machining tools. The wear on a thin film can be simulated by observing the simulated tangential and/or normal forces on an indenter penetrating a thin film or coating. The resistance of coated structures to contact damage is of interest to many engineering applications such as electronic packaging, biomechanics, and aerospace and automotive applications [5, 11, 12]. Ceramics have often been used as coatings on metal substrates because of their many desirable characteristics, such as high hardness and toughness, however the brittleness can become an issue with extended use. Problems such as this have led to the development of coatings based on composite materials.

Recently, composites composed of hard and soft materials, such as ceramics and metals, have been studied. Composites films can be fabricated by layering thin films or embedding metal granules in a hard thin film [13]. By combining the metal and ceramic materials, the most desirable characteristics of both materials can be used. These composite films possess unique mechanical properties. Many of these properties include high strength, hardness and resistance to damage, as well as many other possible functions. Due to the wide use and many possibilities, multilayer thin films have been the subject of many investigations [11, 12, 14–26]. However, uncertainty arises in the characterization of multilayered films using the indentation technique. This is due in large part to the heterogeneity of the material from the layer arrangement of hard/soft material and the number of interfaces associated with the composite. During indentation, the heterogeneous material will not incur the

same sort of stress fields a homogenous material would. The local deformation field will be different from that in a homogenous material, and internal damage may be induced by the indentation loading itself [27, 28]. The effect of material heterogeneity on indentation response (and thus the measurement and interpretation of effective properties extracted from the indentation test) is not well understood. Due to the complicated nature of nanoindentation on multilayered composites, simulating the material in FE software such as ABAQUS, allows multiple different tests to be run without the use of material specimens.

A common composite of layered metal and ceramic is aluminum and silicon carbide (Al/SiC). This combination of materials has been examined in multiple forms. Currently, Al/SiC is specifically being researched for solar physics and optical applications as coating, where it is used for its multiple properties [11, 12]. Recent numerical FE analyses of indentation loading on an aluminum (Al)-silicon carbide (SiC) nanolayered composite found that plastic deformation in the soft Al layers continues to occur during indentation unloading [29–31]. This was attributed to the internal mechanical constraint resulting from the hard SiC layers in the composite structure, as well as a build-up of special stress pattern in the layers. Therefore, the unloading process can no longer be considered to consist of simple recovery of elastic deformation as in a homogeneous material. The unloading induced plasticity was identified by comparing the equivalent plastic strain fields before and after unloading, and by tracking the deformation history of individual material elements in the computational model. There is a need to further investigate this phenomenon, as it has significant implications from both fundamental and practical standpoints. For instance, the unloading-induced plasticity immediately casts doubt on the validity of measuring the elastic modulus of the composite from the unloading response of the indentation.

Composite laminates are vulnerable to failure caused by local transverse stresses.

The resistance of coated structures to contact damage can be studied by combining FE with fracture mechanics [8, 32]. The performance of coatings and thin films is dependent on many different material properties. There is a need to understand the long-term applicability of the film, specifically the fatigue life. Cyclic nanoindentation will be important in determining the fatigue life of composite multilayer thin films. When conducting nanoindentation on a normal material (such as a homogeneous elastic-plastic solid), elastic and plastic deformation is encountered during loading. The elastic strains are recovered in the unloading phase. If the specimen is then cyclically reloaded and unloaded, the load-displacement curve will follow the prior unloading path, which characterizes the elastic nature of the process [33]. Therefore, cyclic indentation response will serve as an indicator for the possible inelastic behavior during the deformation history.

The response of a composite to cyclic indentation is suggestive of its response to damage and fatigue. The cyclic response of homogeneous thin films has recently been experimentally observed in a few studies [34–36]. A numerical cyclic indentation study was conducted on an elastic perfectly plastic material [37]. None of these studies observed the effect of cyclic loading on composite thin films. This research will examine the cyclic indentation response of the Al/SiC nanolayered composite. Nanoindentation, using both FEM and experimental results, will be used to determine the fundamental material characteristics of the layered composite. The specific objectives of this thesis are:

- Gain further insight into unloading induced plasticity in the metal-ceramic system through cyclic indentation modeling,
- Explore the general cyclic indentation load-displacement response, which will also shed light on the contact fatigue behavior of the composite.
- Conduct experimental verification of the model to determine whether the sim-

ulated behavior is in-line with experiments.

Chapter 2

Numerical Model

The composite used in this research consisted of 41 alternating layers of Al and SiC layers on a silicon (Si) substrate. The model used in the simulations corresponds to the multilayer used in the experiments and previous studies [30, 38, 39]. A schematic of the model, with the mesh, is shown in figure 2.1. The mesh of the entire model is shown, and the area around the indenter tip is also included to show the refined mesh at the indentation site.

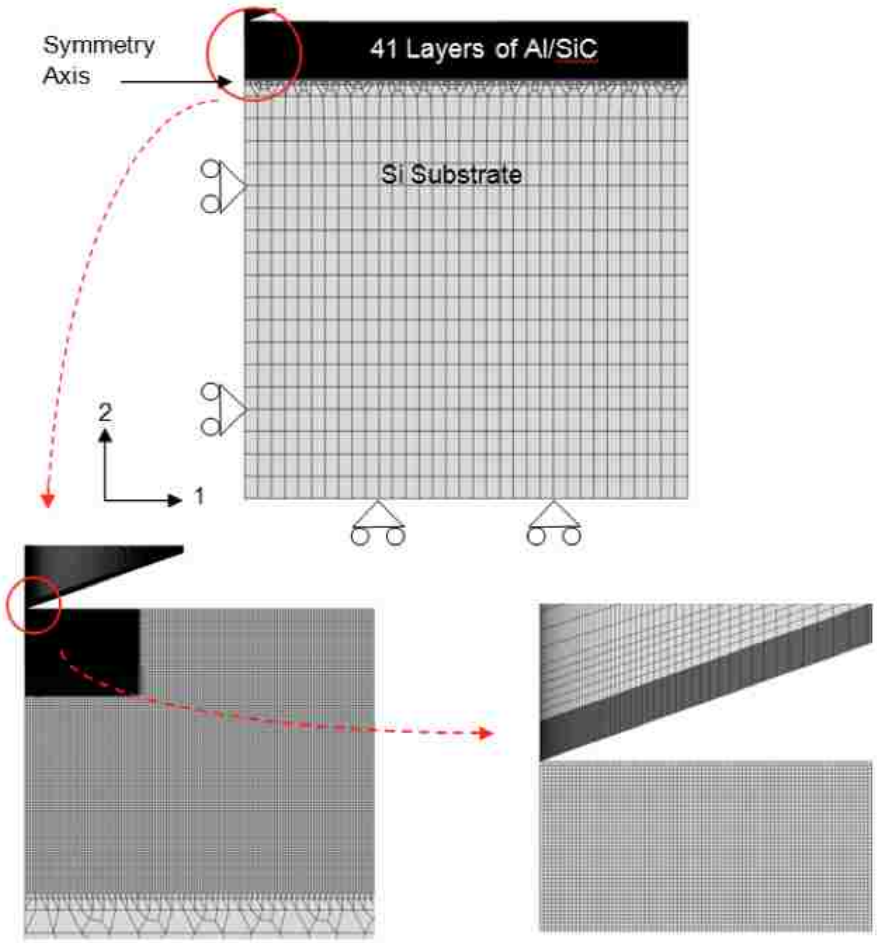

Figure 2.1: Schematic showing the Al/SiC multilayers above a Si substrate, and the boundary conditions used in the axisymmetric model. The finite element mesh near the indentation site is also shown.

In the model, the top layer (in contact with the Al) and the bottom layer (directly above the substrate) are Al. The indentation is modeled with a diamond conical indenter with an angle of 70.3. This represents the same projected indentation area as a Berkovich indenter. Using a conical indenter is practical for use in two-dimensional modeling [1, 9].

The model is axisymmetric, using the left boundary as the symmetry axis. The

entire specimen is 40 μm in lateral span (radius) and 43 μm in height. The individual Al and SiC layers are 50 nm thick. The total thickness of the model is 2.05 μm. The model is constrained so that during indentation, the left boundary can displace in the 2-direction, the bottom boundary is only allowed to move in the 1-direction and the top boundary is free to move. The coefficient of friction between the multilayer and the indenter is assumed to be 0.1. This value is typical for contact between diamond and metal [40, 41]. There are a total of 173,105 linear elements in the model. Each Al and SiC layer is ten elements in thickness. The mesh is more refined in the upper left-hand corner of the model, near the indentation site. The mesh convergence was checked through the modeled indentation load-displacement curves resulting from meshes with different extents of refinement. All analysis was completed using the finite element program ABAQUS (Version 6.10, Dassault Systemes Simulia Corp., Providence, RI).

The Young's moduli for Al and SiC used in the model are 59 GPa and 277 GPa, respectively, which are based on nanoindentation measurements of single-layer Al and SiC films [24]. The Poissons ratios for Al and SiC are taken as 0.33 and 0.17, respectively.

The plastic response of Al is based on the tensile loading data of single-layer Al, with an initial yield strength of 200 MPa. Plastic deformation follows the von Mises criterion with isotropic hardening and the incremental flow theory. The piecewise linear strain hardening response features hardening slopes of 199.3MPa from initial yield up to the strain of 50.5% and then 40.0 MPa up to the strain of 300.7%, beyond which perfect plasticity ensues. This static stress-strain response is used for the plastic strain rate of 1×10-6 s^{-1} and below in the viscoplastic model. The rate-dependent plastic flow strength follows

$$\sigma_e = f\left(\bar{\varepsilon}^p\right) \cdot R\left(\frac{d\bar{\varepsilon}^p}{dt}\right) \tag{2.1}$$

where σ_e is the von Mises effective stress, f (a function of equivalent plastic strain $\overline{\varepsilon}^p$) is the static plastic stressstrain response described above, and R (a function of plastic strain rate $\frac{d\overline{\varepsilon}^p}{dt}$) defines the ratio of flow strength at higher strain rates to the static flow strength where R equals unity. Compared to rate-independent plasticity, this formulation utilizes the scaling parameter R to quantify the strain rate hardening effect. The yield ratio R for Al used in the model is listed in table 2.1 [29]. The SiC ceramic is a much more brittle material. It is nevertheless treated as an elastic-plastic material, with a very high yield point of 8770 MPa (estimated from the indentation hardness of a single-layer SiC film), followed by perfect plasticity. This treatment is necessitated by the fact that a purely elastic SiC in the model will generate unrealistically high loads during the indentation simulation, and is validated by the fact that in the experiment the SiC layers exhibited a glassy/plastic-type response due to the amorphous nature of the film [30]. The Young's modulus and Poissons ratio of the diamond indenter are 1141 GPa and 0.07, respectively. All the interfaces between different materials in the structure are assumed to be perfectly bonded.

Table 2.1: Strain rate hardening response (yield ratios at different plastic strain rates) of Al used in the viscoplastic model

Strain rate (s^-1)	Yield ratio R
1×10^{-6}	1
5×10^{-6}	1.0305
1×10^{-5}	1.0436
5×10^{-5}	1.074
1×10^{-4}	1.0871
5×10^{-4}	1.1176
1×10^{-3}	1.1307
5×10^{-3}	1.1612
1×10^{-2}	1.1743
5×10^{-2}	1.2047
1×10^{-1}	1.2178
5×10^{-1}	1.2483

The cyclic indentation loading was simulated by first pressing the indenter to a depth of 500 nm (ten times the initial layer thickness) for both the control case of a homogenous Al film and the multilayer. The films were then unloaded to 10% of the peak load. Subsequent cycles were then between 10% and 100% of the peak load. The simulations were performed under displacement control, however it was ensured that all load reversals during the cyclic process took place at the chosen maximum and minimum loads.

Chapter 3

Results: Rate-Independent Analyses

For the first part of the research, the evolution of the strain fields in two different thin films was compared. The first case tested was the control case of pure Al on a Si substrate. This is used as the basis for comparison. The second case tested was that of a thin film of alternating layers of Al and SiC on a Si substrate. The FEA results for both cases are compared to experimental data. For this chapter, the loading is considered to be static and no rate dependence is considered in the model.

The maximum load for the Al film was 5.18 mN, which corresponds to a depth of 500 nm during the first indentation loading. Subsequent cycles were then between 10% and 100% of the peak load. For the multilayer, the indentation depth of 500 nm corresponds to an indentation load of 27.5 mN. Unloading to 10% of the peak load, 2.75 mN, then follows.

3.1 Results from Modeling: Control Case

The results for the control case, Al film on a Si substrate, will be presented first. The simulated indentation load-displacement curves for two full cycles is shown in figure 3.1.

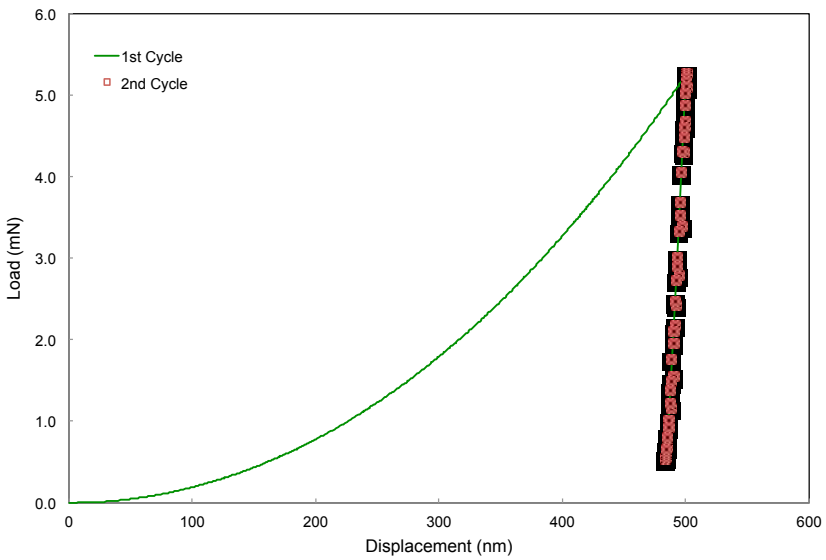

Figure 3.1: Simulated indentation load - displacement curves for the rate - independent control model (2.05 μm thick Al on Si substrate).

The maximum indentation depth, at 500 nm, is approximately $\frac{1}{4}$ of the film thickness. It is observed that both the loading and unloading phases of the second cycle follow the same path as the first unloading response. This indicates the elastic nature of the deformation starting from the first unloading [33]. The manifestation of the elastic deformation can be observed in the equivalent plastic strain. The contour plots of the equivalent plastic strain are shown in figure 3.2. Figure 3.2 (a) and (b) correspond to the beginning and end of the unloading phase in the first cycle, and figure 3.2(c) is after reloading to the peak load. The figures only include the material near the indentation site. As expected, it can be seen that the equivalent

plastic strains remain exactly the same during the process in the homogeneous film material.

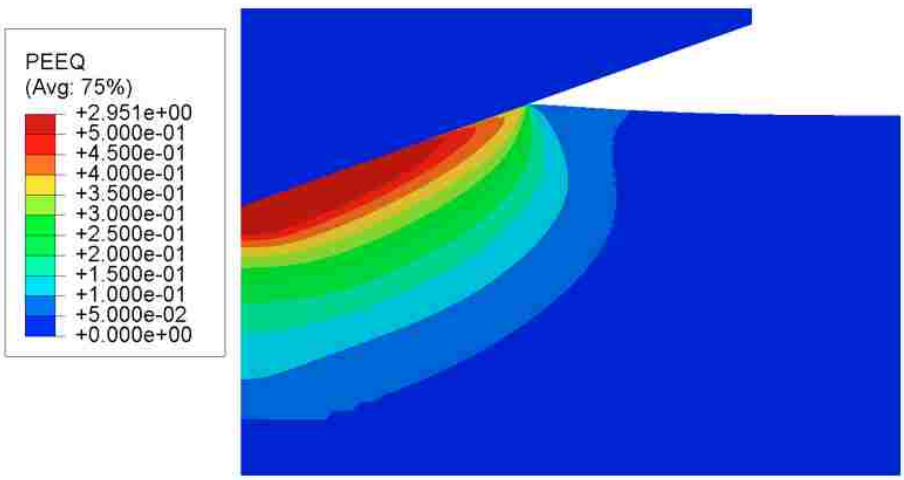
PEEQ
(Avg: 75%)
+2.951e+00
+5.000e-01
+4.500e-01
+4.000e-01
+3.500e-01
+3.000e-01
+2.500e-01
+2.000e-01
+1.500e-01
+1.000e-01
+5.000e-02
+0.000e+00

(a)

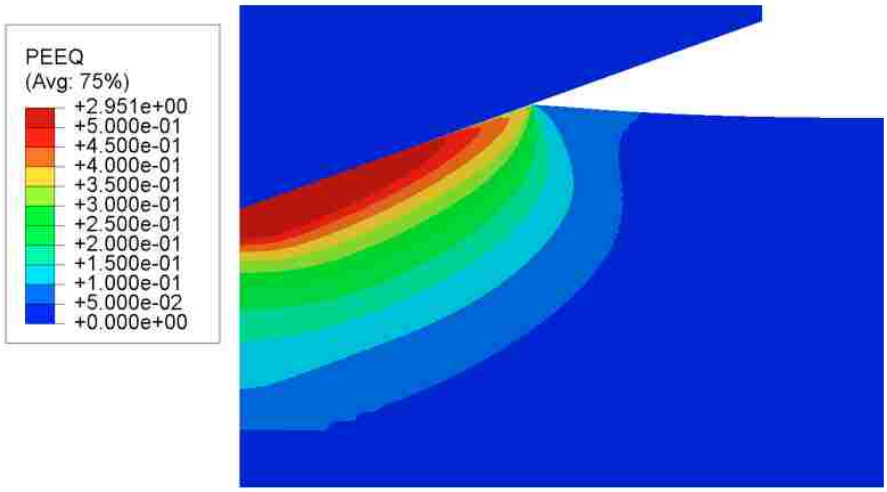
PEEQ
(Avg: 75%)
+2.951e+00
+5.000e-01
+4.500e-01
+4.000e-01
+3.500e-01
+3.000e-01
+2.500e-01
+2.000e-01
+1.500e-01
+1.000e-01
+5.000e-02
+0.000e+00

(b)

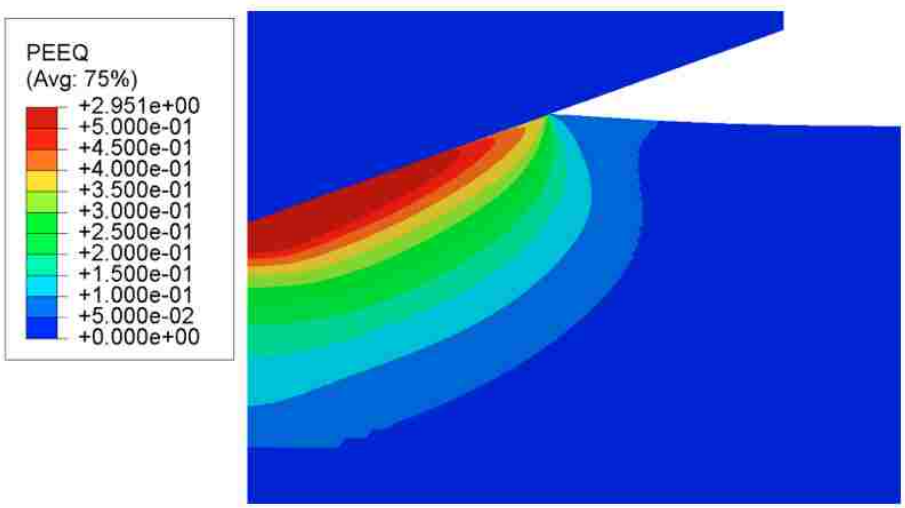

(c)

Figure 3.2: Contour plots of equivalent plastic strain for the case of homogeneous Al film (a) at the peak indentation load after the first loading phase, (b) when the load is reduced to 10% of the peak load after the first unloading, and (c) at the peak loading during the second cycle.

3.2 Results from Modeling: Multilayer

Attention is now turned to the results for the Al/SiC nanolayered composite. Figure 3.3 shows the simulated load-displacement curves for the first two full cycles. Although the maximum indentation depth during the first cycle is the same as in the control case of homogeneous Al film, the peak load is much greater, owing to the much stronger multilayer structure.

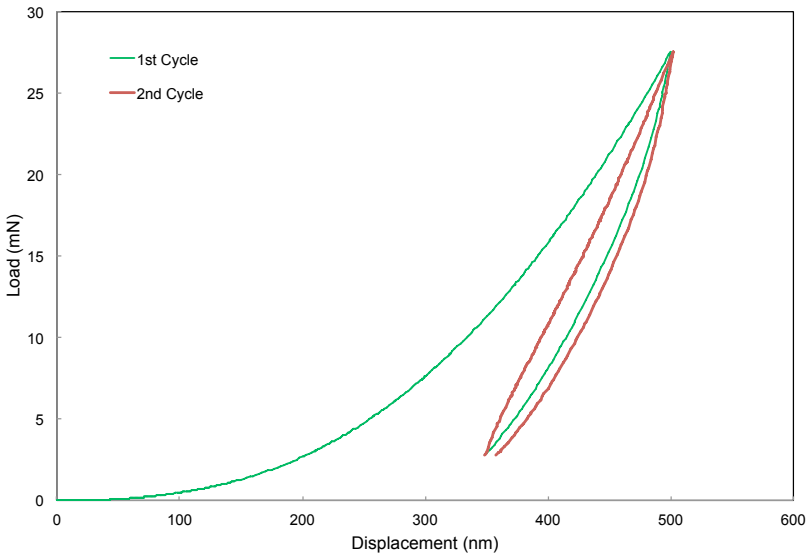

Figure 3.3: Simulated indentation load - displacement curves for the Al/SiC nanolayered composite.).

It is evident from the figure, that unlike the control case, the second cycle does not follow the same path as the first unloading. This indicates the inelastic nature of the deformation process. Furthermore, the open loop nature of the second cycle, indicates that the load-displacement curve is still evolving with continued cycles.

Figures 3.4(a)-(d) show the contour plots of equivalent plastic strain at the first peak load, end of the first cycle, second peak load, and end of the second cycle, respectively. The same legend scale is used in these plots so the strain levels at different stages can be easily compared. In regions where a large contrast in contour levels exists, the deformed laminate geometry can be discerned. Comparing figures 3.4(a) and (b) reveals that plastic strains in the Al layer increase during unloading. The Al layers continue to experience plastic deformation throughout the second cycle, so a continuous increase in plastic strain is seen (figures 3.4(c) and (d)), which contributes to the evolving load-displacement loop seen in figure 3.3.

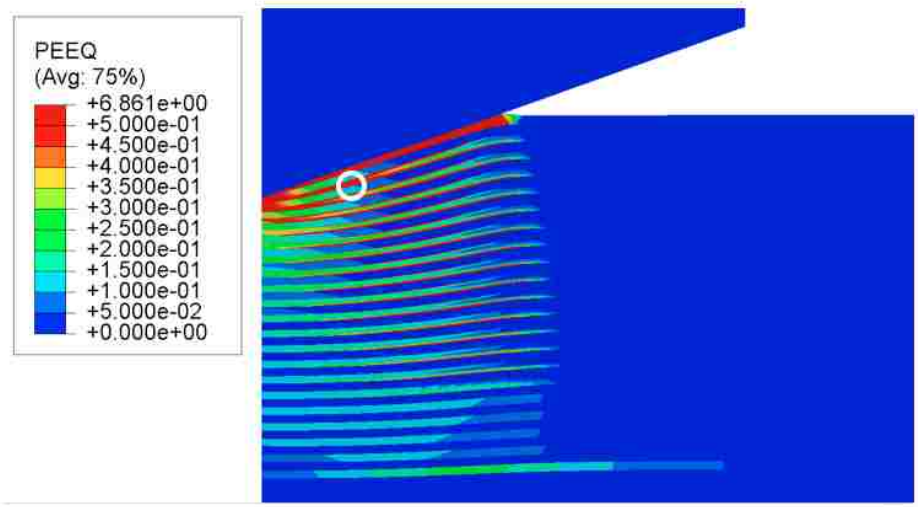
PEEQ
(Avg: 75%)
+6.861e+00
+5.000e-01
+4.500e-01
+4.000e-01
+3.500e-01
+3.000e-01
+2.500e-01
+2.000e-01
+1.500e-01
+1.000e-01
+5.000e-02
+0.000e+00

(a)

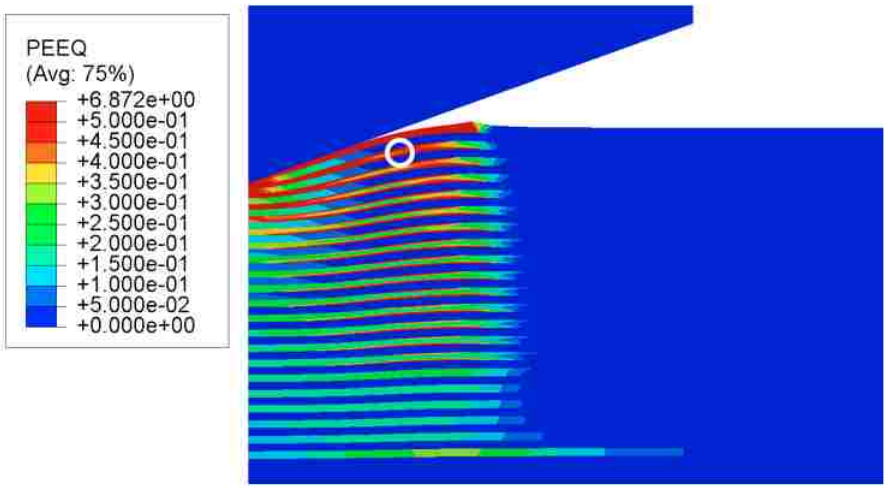
PEEQ
(Avg: 75%)
+6.872e+00
+5.000e-01
+4.500e-01
+4.000e-01
+3.500e-01
+3.000e-01
+2.500e-01
+2.000e-01
+1.500e-01
+1.000e-01
+5.000e-02
+0.000e+00

(b)

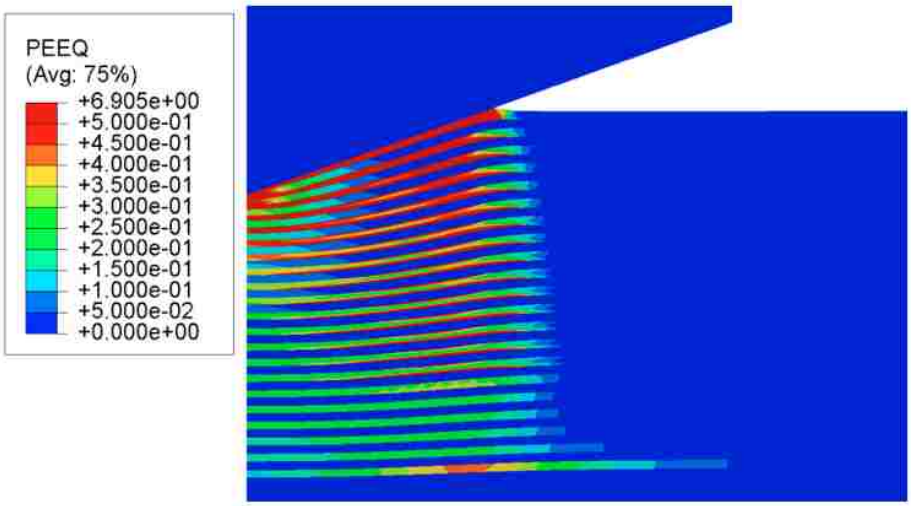

(c)

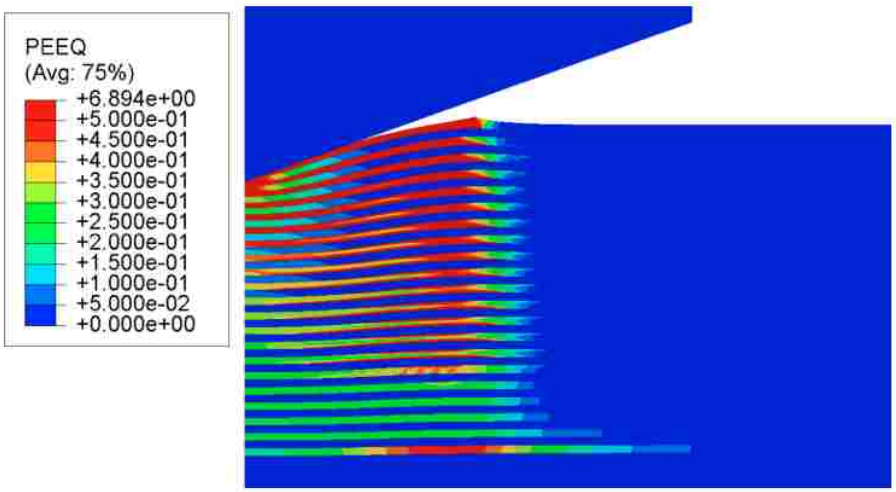

(d)

Figure 3.4: Contour plots of equivalent plastic strain in the Al/SiC nanolayered composite at the following stages: (a) peak load during the first cycle, (b) end of the first cycle, (c) peak load during the second cycle, and (d) end of the second cycle. The white circular marks in (a) and (b) are used for highlighting the locations of material points used in tracking the deformation history as presented in figures 3.5 and 3.6.

To better understand the correlation between cyclic indentation response and

the internal deformation field, the loading/unloading histories of arbitrarily selected material elements in the model were tracked. Two such cases are presented here. The first case refers to the material element inside the second Al layer at a location marked by the circle in figure 3.4(a). Figure 3.5(a) shows the evolution of equivalent plastic strain of this Al element during the first two cycles.

Several stress components (von Mises effective stress VM, normal stresses σ_{11}, σ_{22} and σ_{33}, and shear stress σ_{12}) are shown in figure 3.5(b). It is seen in figure 3.5(a) that equivalent plastic strain increases monotonically. The strain is zero at the beginning of the first loading, when the element is still undergoing elastic deformation. At the end of the first cycle, the plastic strain is at a value well above 0.2. There is a slight pause of plastic strain increase at the initial stage of each unloading and reloading, but plastic deformation soon resumes, with each unloading/reloading phase showing a much higher value at the end compared to the beginning. It is notable, that during each unloading, the total increase in plastic strain is very significant in comparison with the prior loading phase. The evolution of stresses in figure 3.5(b) shows that, during the first loading, large magnitudes of normal compressive stresses along all three directions have developed. At the peak load the magnitude of σ_{22} is greater than σ_{11} and σ_{33} (the indentation direction is along the 2-axis). Upon unloading, the normal stresses rapidly decrease in magnitude. A dip in the Mises effective stress can be seen in the early stages of unloading, which corresponds to the brief period of elastic recovery seen in figure 3.5(a). However, the gradual development of shear stress σ_{12}, along with the combination of other normal stress components, result in the reestablishment of yield condition and thus plastic deformation. The Mises effective stress thus attains the yield value (figure 3.5(b)) and the equivalent plastic strain starts to increase again (figure 3.5(a)). A similar pattern is observed for the second cycle. The second material point also resides in the second Al layer as highlighted in figure3.4(b).

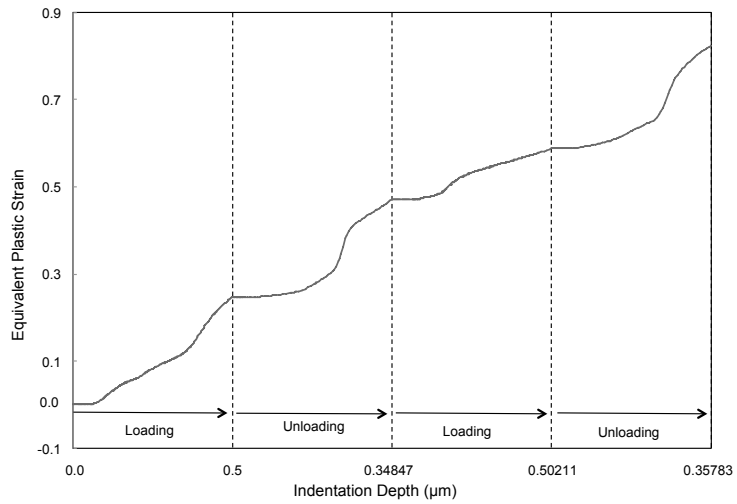

(a)

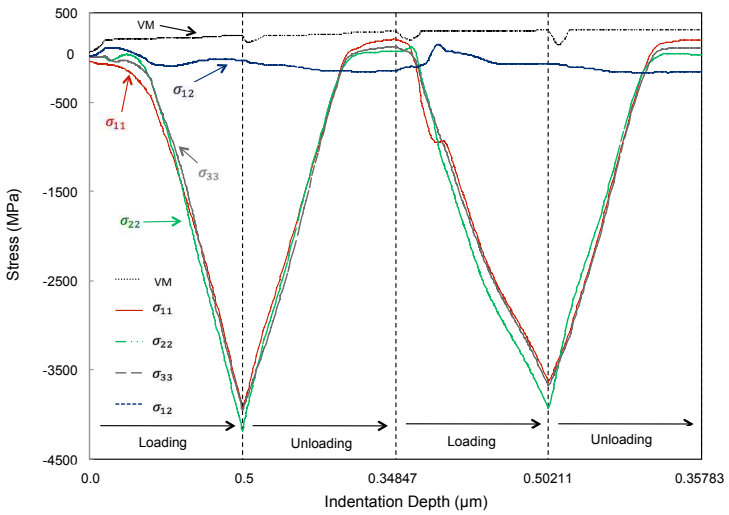

(b)

Figure 3.5: Evolution of (a) equivalent plastic strain and (b) several stress components, in an Al element highlighted in figure 3.4(a), during the first two cycles of deformation history. (VM: von Mises effective stress).

Figure 3.6(a) and (b) show the evolutions of equivalent plastic strain and stress components, respectively, in this element during the first two cycles.

Due to the element's outer location relative to the previous case, the plastic strain

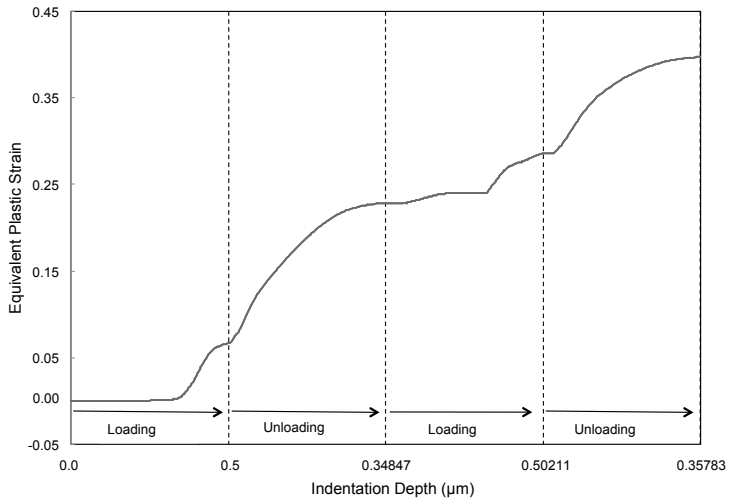

(a)

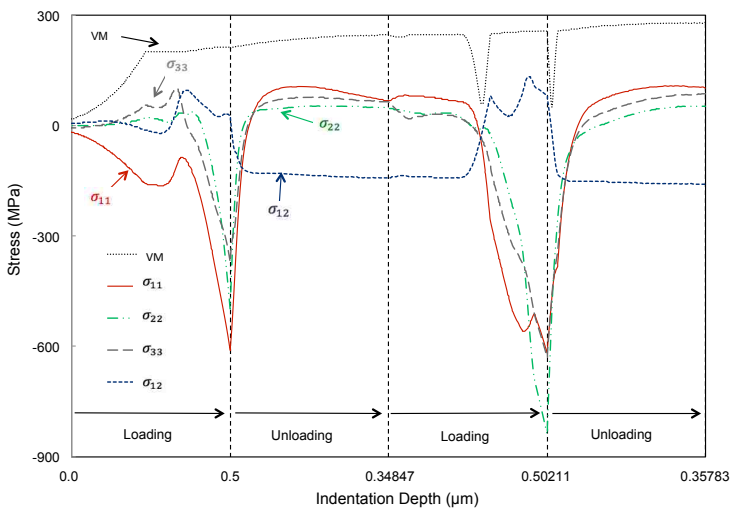

(b)

Figure 3.6: Evolution of (a) equivalent plastic strain and (b) several stress components, in a second Al element highlighted in figure 3.4(b), during the first two cycles of deformation history. (VM: von Mises effective stress).

and normal stress magnitudes are generally smaller. Plastic deformation during each unloading/reloading phase is still evident, and the accumulation of plasticity is much more pronounced during unloading than during loading. In figure 3.6(a),

it is seen that, upon first unloading, there is no elastic recovery period and plastic deformation continues to advance without interruption. This is also evident from the Mises effective stress curve in figure 3.6(b). The Mises effective stress curve remains at the yield value from the first unloading phase through the entire first unloading phase. (The slight increase in the magnitude of Mises stress is due to strain hardening of the Al in the model.) Figure 3.6(b) also reveals that the unloading/reloading induced plasticity in this Al element is generally associated with the development of significant shear stress σ_{12}. There is a rapid increase in its magnitude at the beginning of first unloading, and thereafter the shear stress magnitude stays high when plasticity continues (or reestablishes). Clearly the constraint imposed on the metal by the adjacent hard layers is the primary cause. If uneven deformation occurs in the SiC layers directly above and below, a large shear stress can be easily generated in the Al sandwiched in between.

The indentation beyond two cycles is taken into consideration in figure 3.7. Figure 3.7 shows the simulated load-displacement curves of the Al/SiC multilayered composite for a total of 10 cycles. For the purpose of clarity, the initial part of the first loading curve is not included in the figure.

It is seen that the load-displacement loop of the second cycle persists, although it gradually shifts toward larger displacements. Under a constant load amplitude there is a tendency for the indenter to penetrate deeper as cycling continues. This may be viewed as the indentation version of the cyclic creep phenomenon typically observed under uniaxial loading [42]. It should be noted that the present numerical model only includes rate-independent plasticity, so increasing penetration is not caused by any viscous effect but is purely a consequence of cyclic plasticity under highly constrained conditions. A stabilized loop has not been reached at the end of the tenth cycle. From the evolution of indentation displacement (especially at the minimum load in figure 3.7), a decrease in the advancing rate is evident.

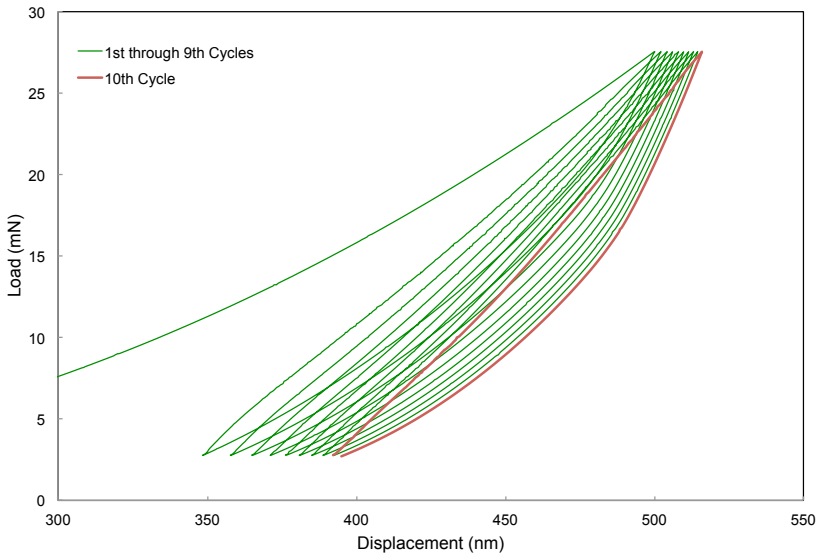

Figure 3.7: Simulated ten full cycles of indentation load-displacement response for the Al/SiC nanolayered composite.

Figures 3.8(a) and (b) show the contour plots of equivalent plastic strain at the end of fifth and tenth cycles, respectively, in the multilayers. It is observed that the plastic strain values are much greater after 10 cycles than after 5 cycles, also showing a significant increase when compared to the first two cycles, seen in figure 3.4.

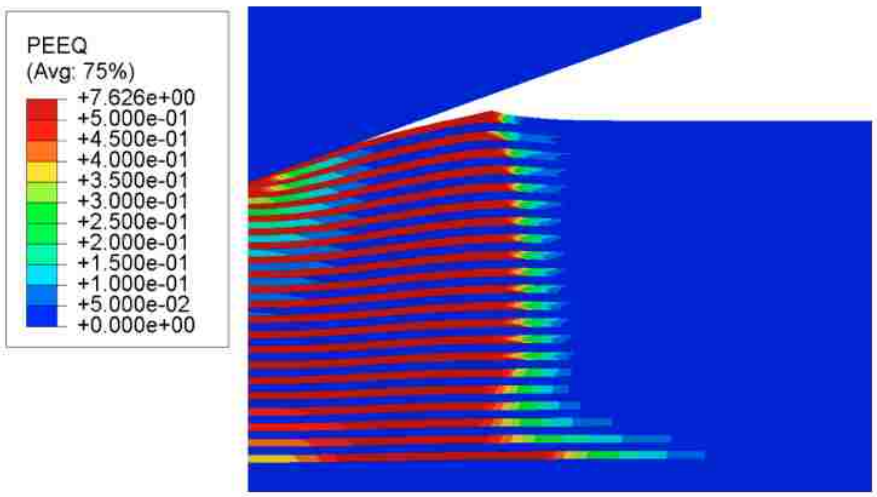

(a)

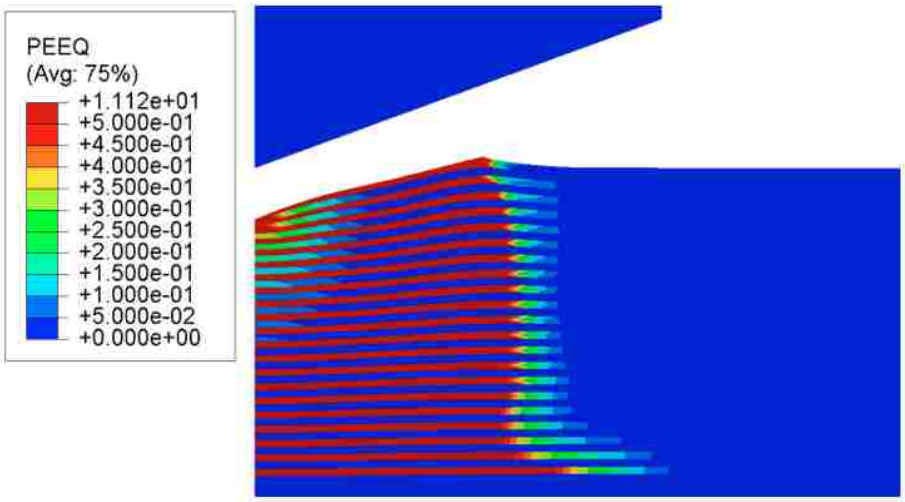

(b)

Figure 3.8: Contour plots of equivalent plastic strain in the Al/SiC nanolayered composite at (a) the end of the fifth cycle and (b) the end of the tenth cycle.

This escalation of plasticity over repeated loading/unloading operations implies the possibility of fatigue crack initiation as a result of further cyclic loading. It is worth pointing out, again, that the continuation of plastic deformation appears

only in the multilayered composite, with the Al layers severely constrained by the SiC layers, but not in the control model with a homogeneous Al film. Therefore, cyclic indentation fatigue damage may become an issue for the type of layered metal/ceramic composite system considered in this study, despite its generally high resistance to monotonic indentation deformation.

3.3 Results from Experiments

This section presents the experimental measurements of the cyclic nanoindentation response, conducted by collaborators at Arizona State University. The Al and SiC layers were synthesized by physical vapor deposition (magnetron sputtering) on a (111) single-crystal Si substrate [27, 28, 30]. The base pressure of the dual-gun sputtering chamber was approximately 10^{-7} Torr (1.33×10^{-7}Pa). Targets of pure Al (99.99%) and SiC (99.5%) (Kurt Lesker, Clairton, PA) were used for sputtering in argon atmosphere, at an argon pressure of about 3 mTorr (0.4 Pa). The Al was sputtered using a DC sputter gun with a power of 95 W while the SiC was sputtered by a RF sputter gun at 215 W. The targets were pre-sputtered for about 10 min at 40 W for Al and 95 W for SiC to remove any oxides and impurities from the surface. Under these conditions, the deposition rates were 7.5 nm/min and 3.9 nm/min for Al and SiC, respectively. Twenty-one layers of alternating Al and SiC with a nominal layer thickness of 50 nm were produced. The Al layers have a columnar grain structure with an average grain length slightly greater than the layer thickness, and the SiC layers are amorphous. In addition, a control specimen of a 1000 nm-thick Al film on a Si substrate was also used.

Nanoindentation was conducted using a commercial nanoindenter (Nano-XP, Agilent, Chandler, AZ). The maximum loads for the Al/SiC composite and single-layer Al were 49 mN and 6.0 mN, respectively. These peak loads resulted in maximum

indentation displacements around 500-600 nm (i.e., approximately 10-12 layer thicknesses in the case of composite). As in the modeling, cyclic loading was conducted between 10% and 100% of the peak load.

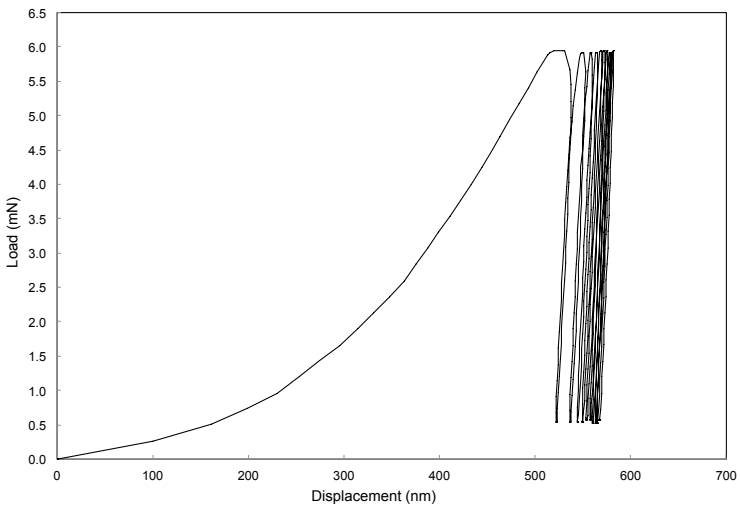

(a)

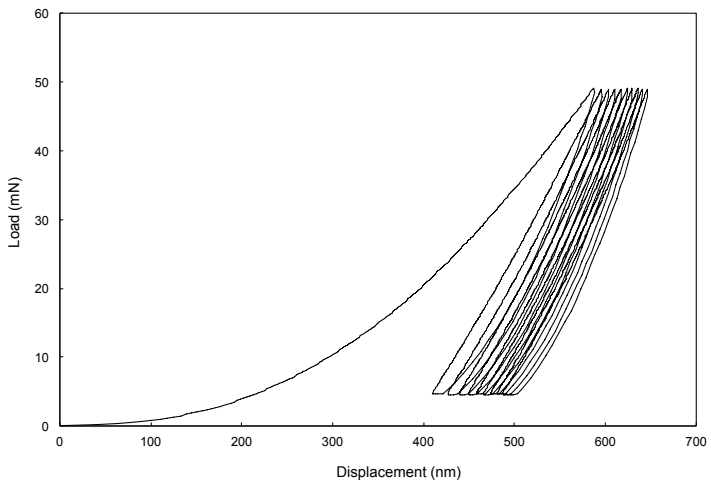

(b)

Figure 3.9: Experimentally measured cyclic nanoindentation load-displacement response of (a) the control specimen (with a thick Al film) and (b) the Al/SiC nanolayered composite.

Figure 3.9(a) shows the experimental result of the control specimen. There is drift toward larger displacements starting from the first loading phase, which is due to the time-dependent behavior that is frequently observed in metallic thin films under indentation. The result is qualitatively similar to a cyclic indentation measurement on a bulk Al specimen [36]. Figure 3.9(a), however, also shows that stabilization was reached after several cycles, and subsequent reloading and unloading followed the same load-displacement path. This signifies elastic deformation as illustrated in the numerical modeling shown in figure 3.1, where the much steeper unloading curve compared to the composite is also in agreement with the experiment.

Figure 3.9(b) shows the measured load-displacement curves of the Al/SiC composite for 10 cycles. The same deformation features occur as in the modeling (figure 3.7), i.e., progressive open loops toward deeper penetrations over the cycles. The inelastic nature of the unloading/reloading response is evident, and the deformation has not reached stabilization after 10 cycles.

Although it may be conceived that the displacement drift displayed by the Al/SiC multilayers may also be aided by the viscous response of Al films, the cyclic hysteresis loops in figure 3.9(b) clearly contrasts with the stabilized elastic behavior displayed by the nearly linear unloading curve seen in figure 3.9(a).

Furthermore, previous experimental and numerical studies on viscoplastic deformation of Al/SiC nanolayers have demonstrated that the time-dependent nature of Al is greatly suppressed in the case of multilayers [43]. It is concluded that plastic deformation during the recurring unloading/reloading process is a distinct feature of the layered composite.

3.4 Conclusions

A systematic modeling study on cyclic indentation response of the Al/SiC nanolayered composite was carried out. It showed that plastic deformation in the ductile Al layers continues to occur during the unloading phase of the first cycle, as well as during subsequent reloading/unloading processes. The cyclic plasticity results in an open load-displacement loop, and the maximum indentation depth continues to increase with each cycle under a constant load amplitude. Tracking the deformation history of individual material elements provided insight on how the deformation in the soft metal is constrained by the adjoining hard layers. The recurring plastic deformation is not seen in the control model of a homogeneous Al film, where load-displacement curves during cycles simply followed the first unloading path. The modeling result raises the issue of possible indentation fatigue damage in the layered composite. Nanoindentation experiments under the same type of cyclic loading condition also showed the evolving load-displacement loops, in qualitative agreement with the modeling.

Chapter 4

Results: Rate-Dependent Analyses

In this chapter the rate-dependence of the Al film is taken into consideration, for gaining insight on how the viscoplastic characteristics of the Al layers can affect the cyclic indentation response. Again, there was the control case of pure Al on a Si substrate, and a thin film of alternating layers of Al and SiC on a Si substrate. The FEA results for both cases are compared to experimental data.

At a depth of 500 nm, the maximum indentation load for the multilayer is 28.2 mN. Unloading to 10% of the peak load, 2.82 mN, then followed. The following cycles were then carried out between the maximum and minimum loads. The same type of deformation history was also applied to a control model. In this case the peak load is 6.30 mN, which corresponds to a depth of 500 nm during the first indentation loading. Subsequent cycles were then between approximately 10% and 100% of the peak load. Both loading and unloading were simulated under a constant rate of 2000 nm/s, with no hold period at the maximum and minimum loads. In the presentation of results below, the differences between the control model and the multilayered model will be emphasized.

4.1 The First Two Cycles

The modeling results of the first two indentation cycles are presented first. Figure 4.1 shows the simulated indentation load-displacement curves for the control model (thick Al film on Si substrate). The maximum indentation depth, 500 nm, is at approximately $\frac{1}{4}$ of the film thickness.

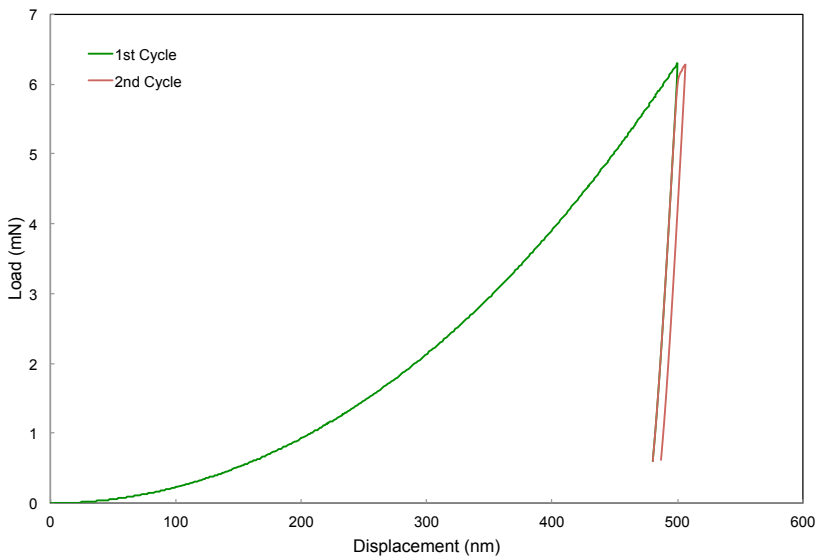

Figure 4.1: Simulated indentation load - displacement curves for the rate - dependent control model (2.05 μm thick Al on Si substrate).

It can be seen that, after the first unloading phase, reloading follows the same path as the first unloading until very close to the peak load. The indenter then penetrates deeper into the material. This observation suggests that, for the most part, the unload/reload action is a repetitive elastic process. Near the end of the reloading, further inelastic deformation occurs which is a consequence of the rate-dependent viscoplastic behavior. (If only rate-independent plasticity is used for Al, the unload/reload response follows exactly the same track in the entire load range as seen in chapter 3 [38].) The second unloading curve appears to be parallel to the

first unloading.

Figure 4.2 shows the simulated load-displacement curves of the Al/SiC nanolayered composite. Although the maximum indentation depth during the first cycle is the same as in the previous case of a thick homogeneous Al film, the peak load is much greater in figure 4.2 due to the much stronger metal/ceramic composite structure.

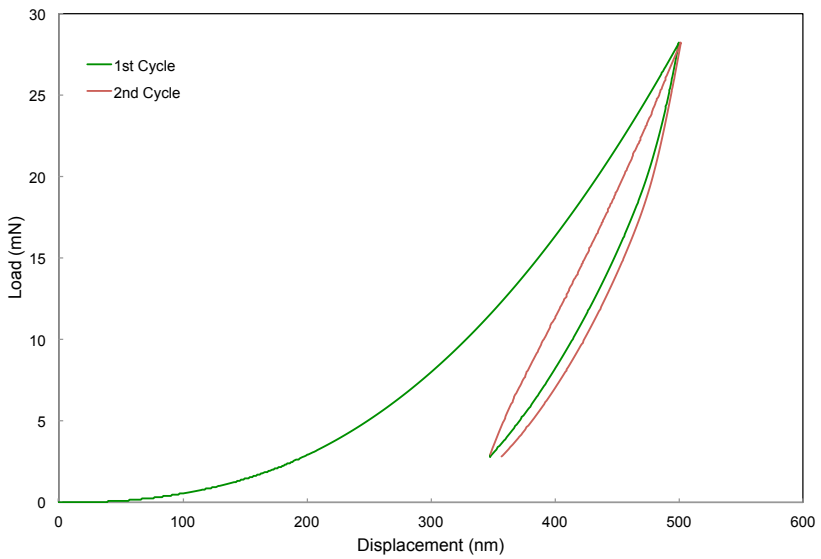

Figure 4.2: Simulated indentation load - displacement curves for the Al/SiC nanolayered composite.

It is evident that the second cycle, even as it starts, does not follow the same path as the first unloading, which indicates the inelastic nature of the deformation process. Furthermore, as seen in chapter 3, the second cycle leads to an open hysteresis loop, implying that the load-displacement response is still evolving if cycling continues.

Figures 4.3(a) and (b) show the contour plots of equivalent plastic strain, in the control model, at the beginning and end of the unloading phase in the first cycle, respectively. Only the material near the indentation site is included in the

presentation. The plastic strain field is seen to remain unchanged during unloading. Figure 4.3(c) shows the contour plot corresponding to the end of reloading (i.e., the peak point in the second cycle). Compared to figure 4.3(b), there is a slight increase in plasticity in 4.3(c) (manifested by the slight expansion of high-strain colors). This expansion is due to the viscoplastic effect at high loads near the end of the reloading (figure 4.1), which will be further elaborated below.

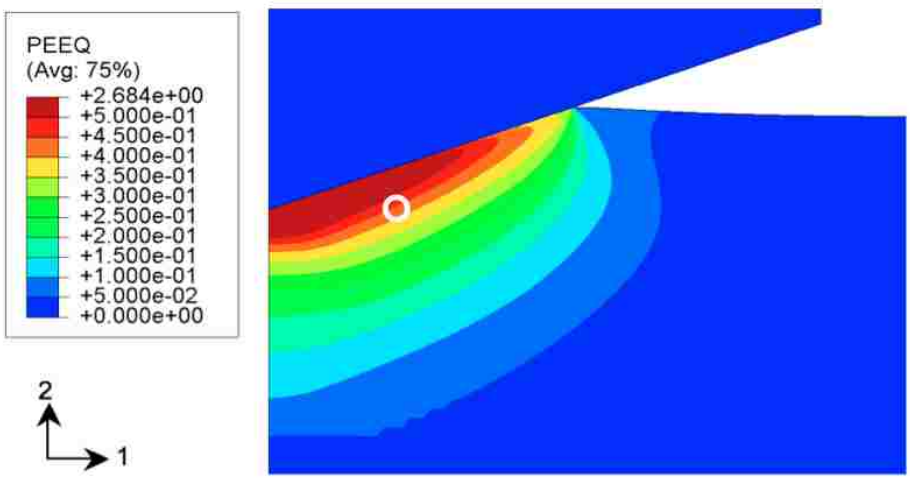
PEEQ
(Avg: 75%)
+2.684e+00
+5.000e-01
+4.500e-01
+4.000e-01
+3.500e-01
+3.000e-01
+2.500e-01
+2.000e-01
+1.500e-01
+1.000e-01
+5.000e-02
+0.000e+00
2
1

(a)

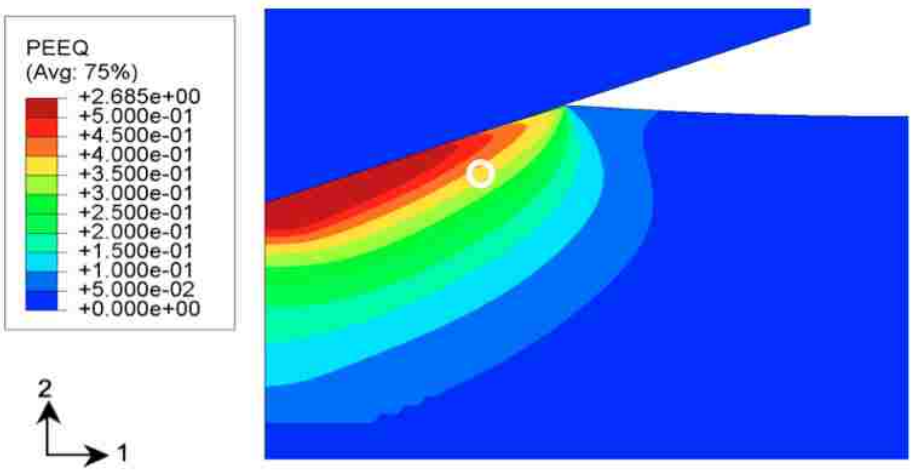
PEEQ
(Avg: 75%)
+2.685e+00
+5.000e-01
+4.500e-01
+4.000e-01
+3.500e-01
+3.000e-01
+2.500e-01
+2.000e-01
+1.500e-01
+1.000e-01
+5.000e-02
+0.000e+00
2
1

(b)

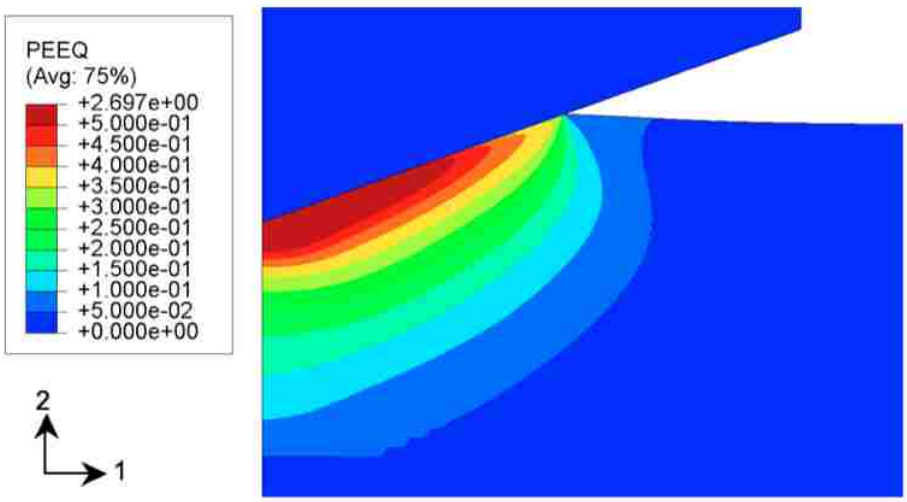

(c)

Figure 4.3: Contour plots of equivalent plastic strain (denoted as PEEQ) for the case of a homogeneous Al film (a) at the peak indentation load after the first loading phase, (b) when the load is reduced to 10% of the peak load after the first unloading, and (c) at the peak loading during the second cycle. The white circular marks in (a) and (b) are used for highlighting the locations of material points used in tracking the deformation history as presented in figure 4.5 and figure 4.6

Figures 4.4(a)-(d) show the contour plots of equivalent plastic strain at the first peak load, end of the first cycle, second peak load, and end of the second cycle, respectively, in the Al/SiC multilayers. The same legend scale is used in these plots so the strain levels at different stages can be easily compared. A comparison between figures 4.4(a) and (b) reveals that plastic strains in Al have increased significantly, due to the pure unloading process. In fact, throughout the second cycle the Al layers continue to experience plastic deformation so a continuous increase in plastic strain is seen (figure 4.4(c) and (d)), which contributes to the evolving load-displacement loop observed in figure 4.2.

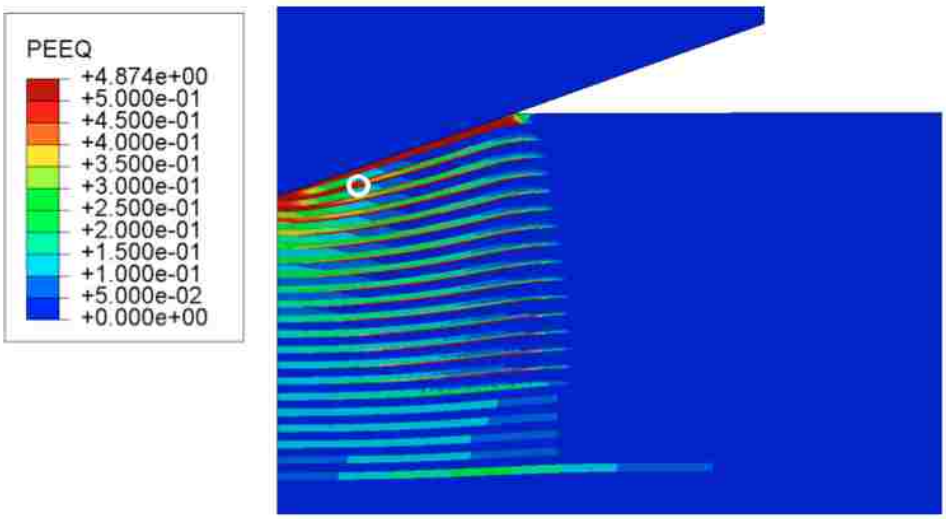
PEEQ
+4.874e+00
+5.000e-01
+4.500e-01
+4.000e-01
+3.500e-01
+3.000e-01
+2.500e-01
+2.000e-01
+1.500e-01
+1.000e-01
+5.000e-02
+0.000e+00

(a)

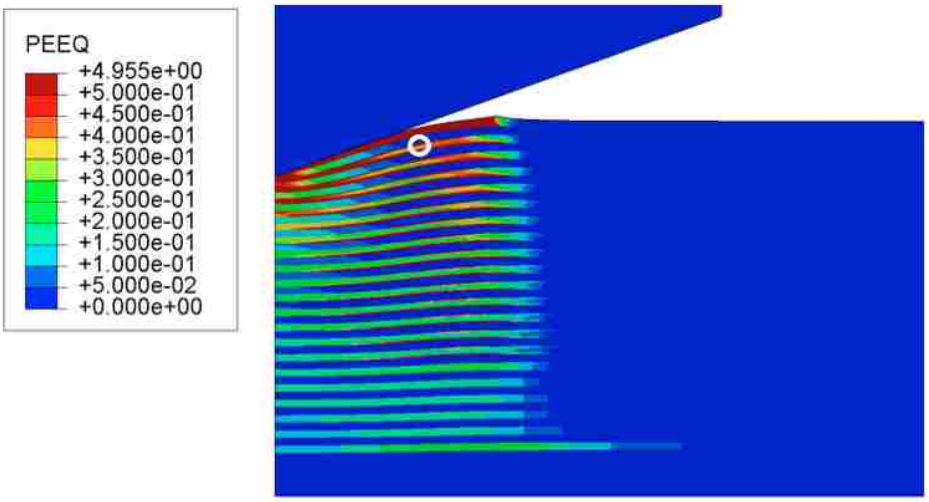
PEEQ
+4.955e+00
+5.000e-01
+4.500e-01
+4.000e-01
+3.500e-01
+3.000e-01
+2.500e-01
+2.000e-01
+1.500e-01
+1.000e-01
+5.000e-02
+0.000e+00

(b)

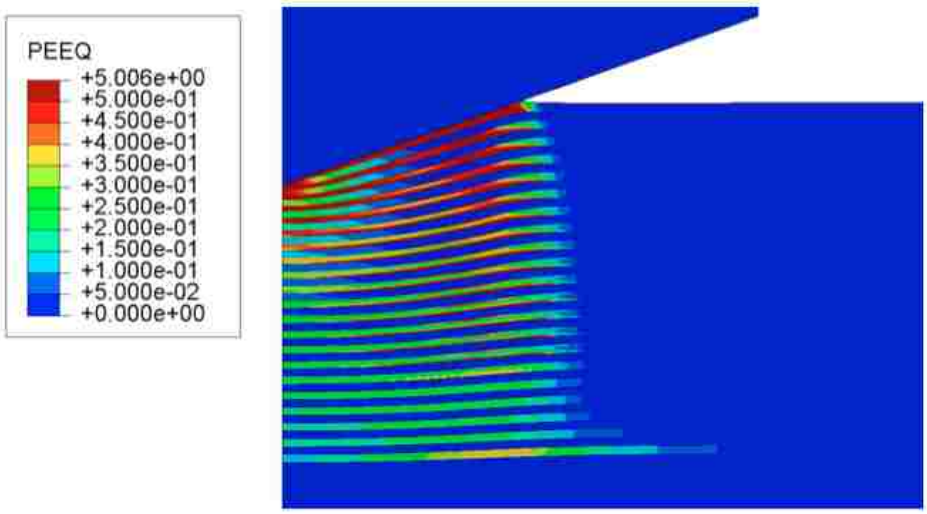

(c)

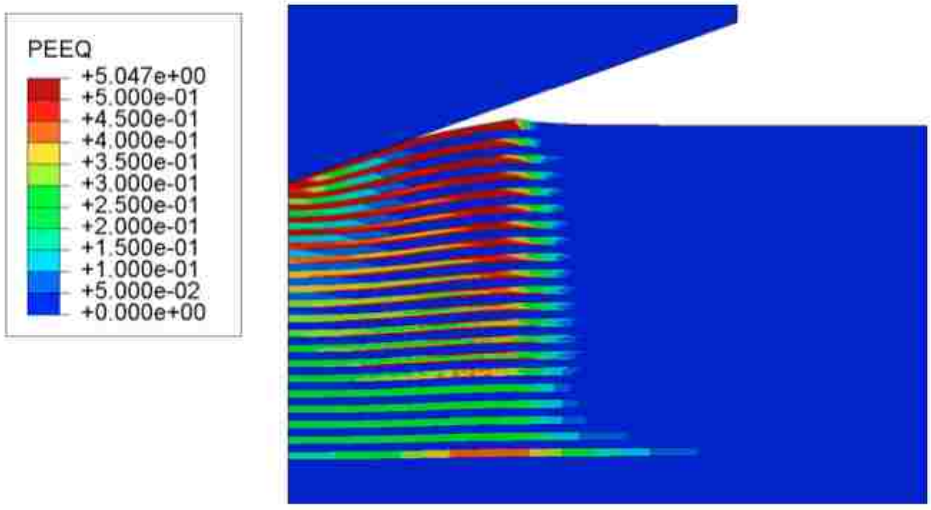

(d)

Figure 4.4: Contour plots of equivalent plastic strain (denoted as PEEQ) in the Al/SiC nanolayered composite at the following stages: (a) peak load during the first cycle, (b) end of the first cycle, (c) peak load during the second cycle, and (d) end of the second cycle. The white circular marks in (a) and (b) are used for highlighting the locations of material points used in tracking the deformation history as presented in figure 4.7 and figure 4.8

4.2 Tracking of Deformation Histories

To better understand the correlation between cyclic indentation response and the internal deformation field, the loading/unloading histories of arbitrarily selected material elements in the model were followed. Attention is devoted to the control model first, with two cases presented here. The first case is an element inside the highlighted circle in figure 4.3(a). Figure 4.5(a) shows the evolution of equivalent plastic strain of this element during the first two cycles. The corresponding plot for several stress components (von Mises effective stress VM, normal stresses σ_{11}, σ_{22} and σ_{33}, and shear stress σ_{12}) is shown in figure 4.5(b).

It can be seen in figure 4.5(a) that the equivalent plastic strain increases drastically during the first loading. Near the peak displacement the various stress components appear to reach saturated values (figure 4.5(b)), with large differences between σ_{22} and the other two normal components, thus giving rise to large deviatoric values for plastic flow. Upon unloading the equivalent plastic strain remains the same, signifying that the element is undergoing elastic recovery. During loading in the second cycle, the plastic strain remains constant before it increases (slightly) again toward the end of the reloading. The stress components also attain similar values near the end of the initial loading. Apparently the reestablished stress state, coupled with the viscoplastic nature of the material, promote creep deformation near the second peak load. This evolution of local deformation history is consistent with the overall indentation behavior observed in figures 4.1 and 4.3.

The second material element chosen is situated toward the outer direction, the position of which is highlighted in figure 4.3(b). The evolutions of the equivalent plastic strain and stress components are shown in figure 4.6(a) and (b), respectively. Due to its outer location, this element experiences lower plastic strain and normal stresses. Nevertheless, the same general trend as in figure 4.5 is observed. One

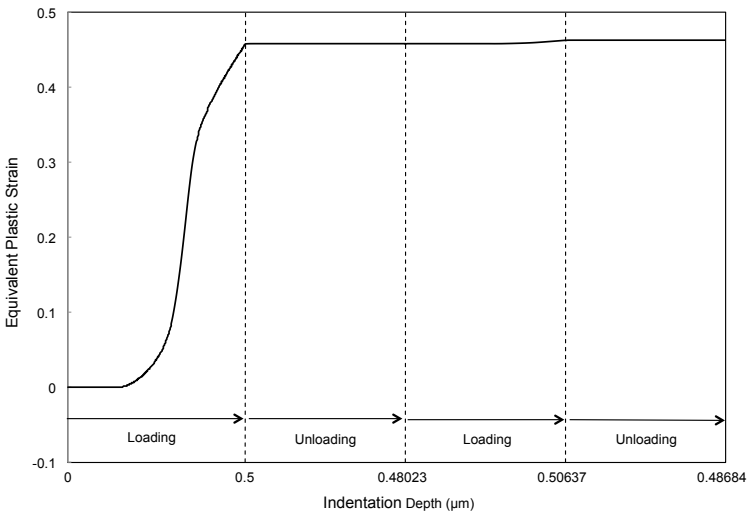

(a)

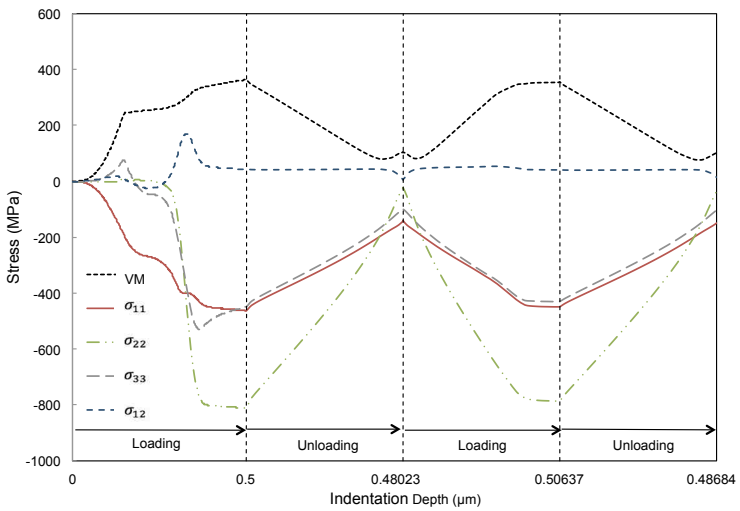

(b)

Figure 4.5: Evolution of (a) equivalent plastic strain and (b) several stress components, in an element highlighted in figure 4.3(a), during the first two cycles of deformation history. (VM: von Mises effective stress).

notable feature is that, in figure 4.5(b), the shear stress has relatively small value and is quite steady after the first loading. In figure 4.6(b), however, the change in σ_{12} with indentation history is more severe. This is again due to the fact that the

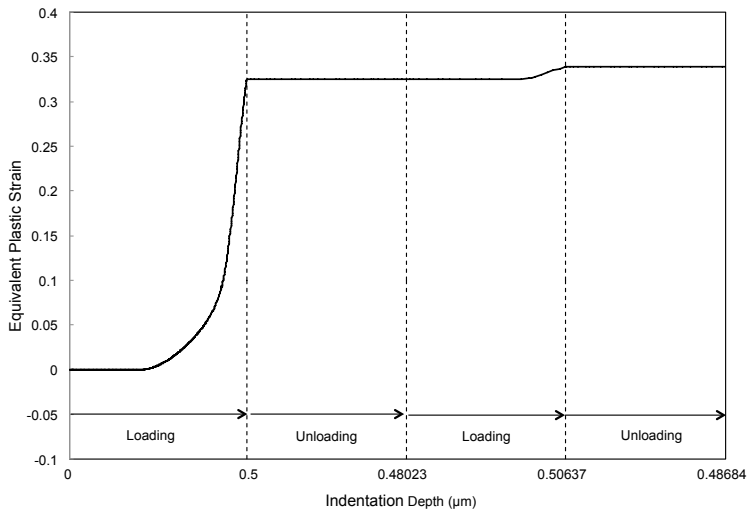

(a)

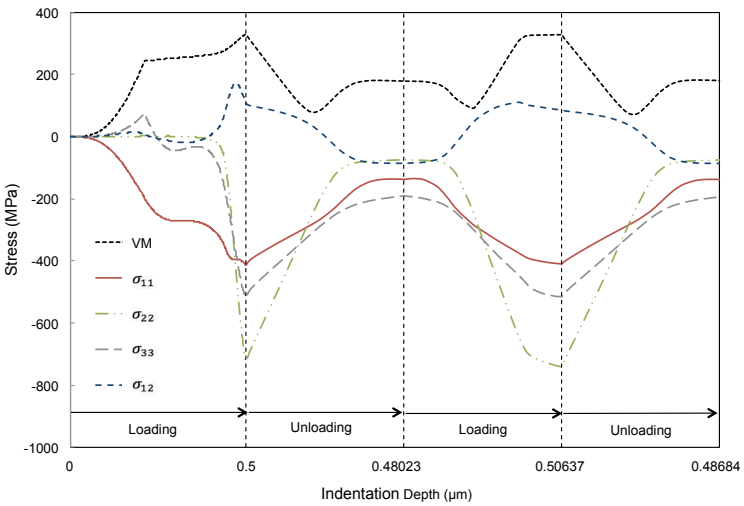

(b)

Figure 4.6: Evolution of (a) equivalent plastic strain and (b) several stress components, in a second element highlighted in figure 4.3(b), during the first two cycles of deformation history. (VM: von Mises effective stress).

element in figure 4.6 is closer to the indentation edge, so the load/unload action exerts greater influence on its shear stress state.

The local deformation history in the Al/SiC multilayers is now considered. The

first tracked element is inside the second Al layer at a location marked by the circle in figure 4.4(a). Figure 4.7(a) and (b) show the evolutions of equivalent plastic strain and stress components, respectively, during the first two cycles.

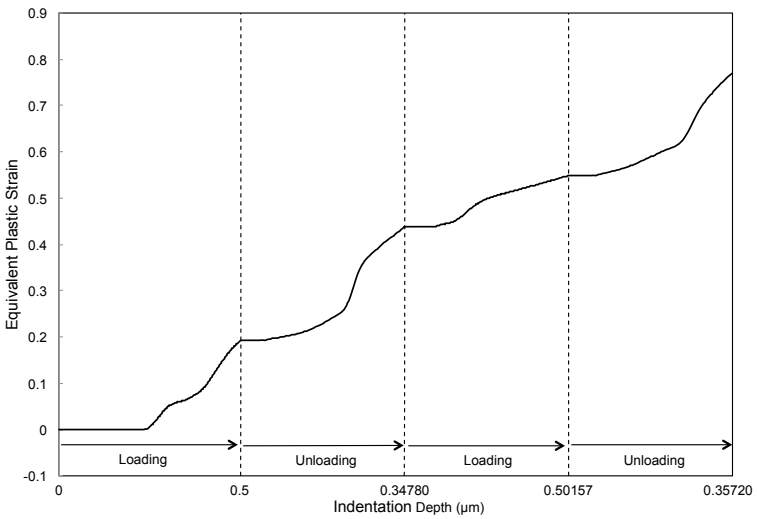

(a)

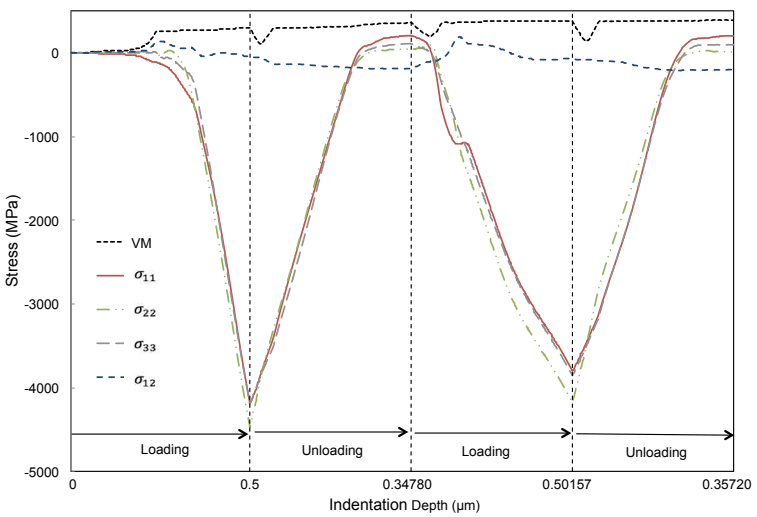

(b)

Figure 4.7: Evolution of (a) equivalent plastic strain and (b) several stress components, in an Al element highlighted in figure 4.4(a), during the first two cycles of deformation history. (VM: von Mises effective stress).

It can be seen in figure 4.7(a) that equivalent plastic strain increases monotonically. There is a pause of plastic strain increase at the initial stage of each unloading and reloading, but plastic deformation soon resumes, with each unload/reload phase showing a much higher value at the end compared to the beginning. Figure 4.7((b) shows that, during the first loading, large magnitudes of normal compressive stresses have developed. Upon unloading, the normal stresses rapidly decrease in magnitude. A dip in the Mises effective stress can be seen, corresponding to the brief period of elastic recovery seen in figure 4.7((a). However, the gradual development of shear stress σ_{12}, along with the combination of other stress components, results in the reestablishment of yield condition and thus plastic deformation at an early stage of the unloading phase. A similar pattern is observed for the second cycle.

The second material point considered for the Al/SiC multilayers also resides in the second Al layer as highlighted in figure 4.4(b). Figures 4.8(a) and (b) show the evolutions of equivalent plastic strain and stress components, respectively, in this element during the first two cycles. At this outer position the plastic strain and normal stress magnitudes are generally smaller. Plastic deformation during each unload/reload phase is still evident. It can be seen in figure 4.8(a) that, upon first unloading, there is a very brief elastic recovery period and plastic deformation soon advances again. This is also evident from the Mises effective stress curve in figure 4.8(b). (The slight increase in the magnitude of Mises stress, in both figures 4.7(b) and 4.8(b), is due to strain hardening in the model.) Figure 4.8(b) also reveals that the unload/reload-induced plasticity in this Al element is generally associated with the development of significant magnitudes of shear stress σ_{12}. The effect on the metal by the hard adjacent layers is the cause. These results are very similar to those of the multilayer model presented in chapter 3.

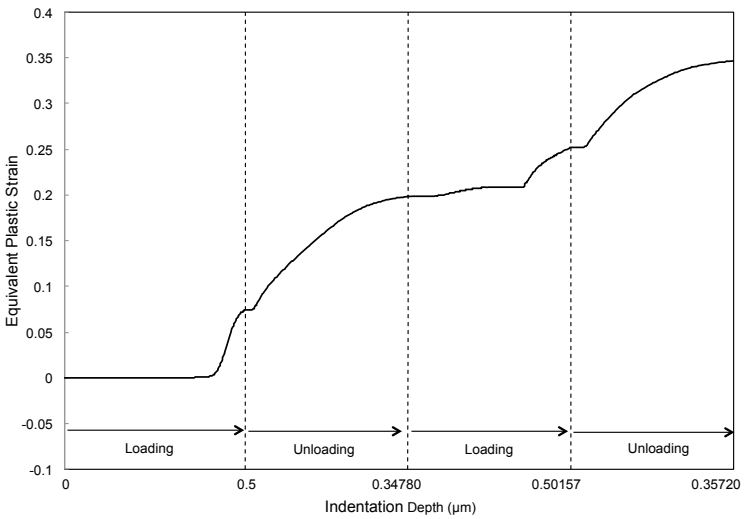

(a)

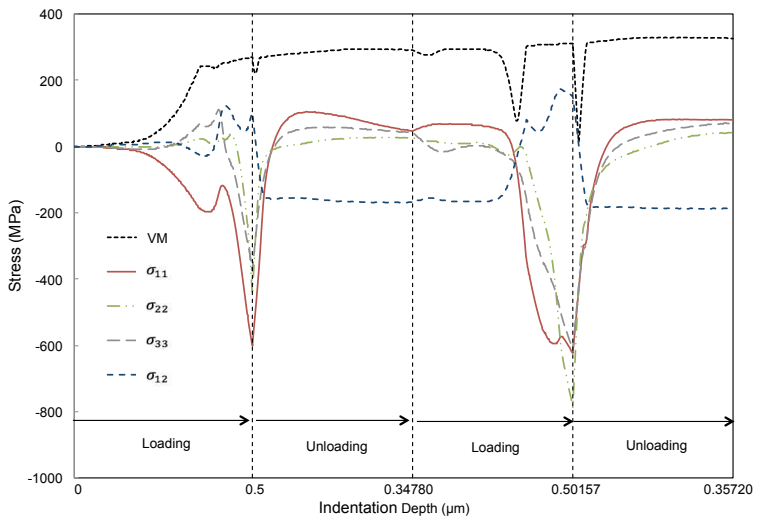

(b)

Figure 4.8: Evolution of (a) equivalent plastic strain and (b) several stress components, in a second Al element highlighted in figure 4.4(b), during the first two cycles of deformation history. (VM: von Mises effective stress).

On the basis of the evolution of deformation history considered above, it is understood that the primary difference between the layered structure and the control model lies in the extent of resumed plasticity. Significant plastic deformation contin-

ues to occur in the Al/SiC multilayers during each of the unload and reload phases. For the homogeneous Al film, pure elastic recovery takes place during unloading while there is only a slight gain of plastic strain at the end of reloading.

4.3 Beyond the Second Cycle

The indentation response beyond the first two cycles is presented below. Figure 4.9 shows the simulated load-displacement curves of the control model for a total of ten full cycles. The beginning of the initial loading has been excluded from the presentation for clarity. As the cycles accumulate, the indenter penetrates deeper into the metal but its rate is decreasing. In other words, cyclic indentation is moving toward stabilization as the reloading-generated viscoplastic deformation gradually diminishes.

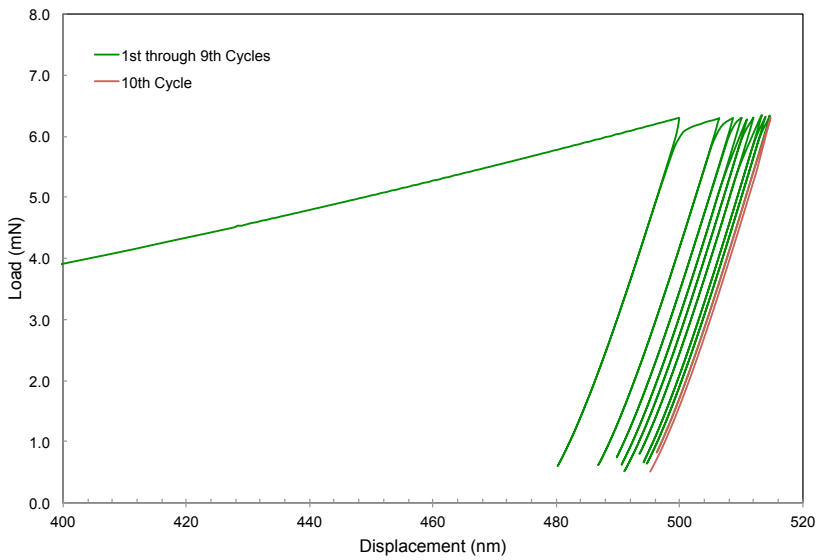

Figure 4.9: Simulated ten full cycles of indentation load-displacement response for the homogeneous Al film.

Figure 4.10 shows the simulated load-displacement curves of the Al/SiC nanolayered composite for a total of six cycles. It can be seen that the load-displacement loop of the second cycle persists, with a gradual shift toward larger displacements. As in the control case, under a constant load amplitude there is a tendency for the indenter to penetrate deeper as cycling continues. From the evolution of indentation displacement (especially at the minimum load in figure 4.10), a decrease in the advancing rate is evident. The main difference from the control model, however, is the distinct hysteresis loops caused by the continued plastic deformation during the unloading and reloading operation in the case of Al/SiC multilayers.

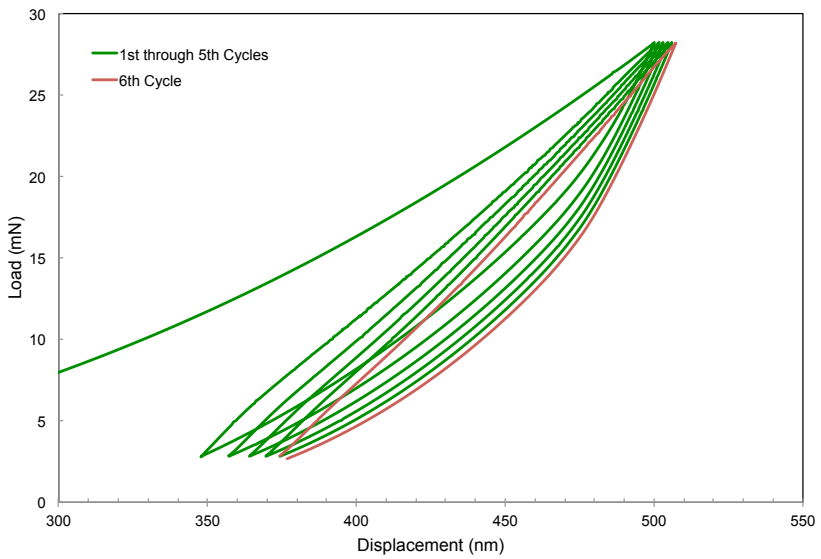

Figure 4.10: Simulated cyclic indentation load - displacement response for the Al/SiC nanolayered composite.

Figures 4.11(a) and (b) show the contour plots of equivalent plastic strain at the end of the third and sixth cycles, respectively, in the multilayers. It is observed that the plastic strain values are much greater after six cycles than after three cycles (which in turn shows a significant increase compared to the first two cycles, figure 4.4). This escalation of plasticity over repeated load/unload operations implies the

possibility of fatigue crack initiation as a result of further cyclic loading, as mentioned in chapter 3. Therefore, damage due to contact fatigue [42] may become an issue for the type of layered metal/ceramic composite system considered in this study, despite its generally high resistance to monotonic indentation deformation.

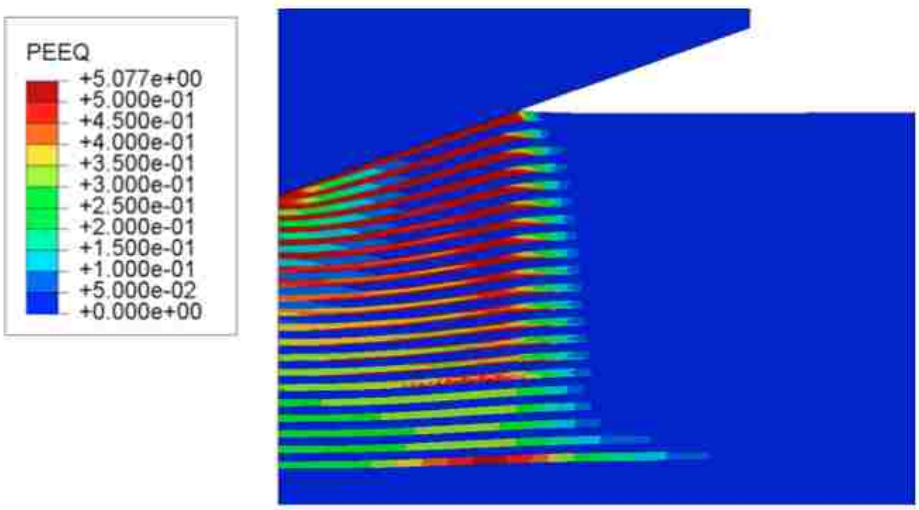

(a)

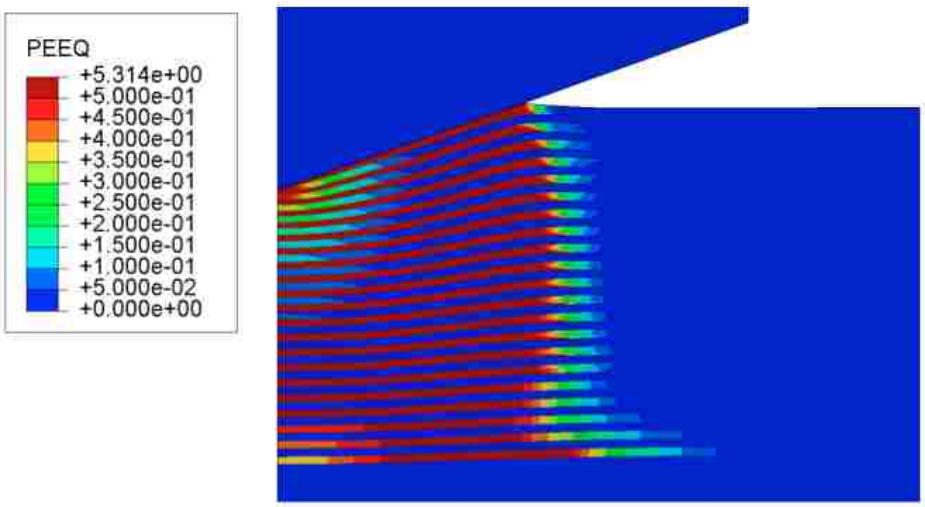

(b)

Figure 4.11: Contour plots of the equivalent plastic strain (denoted as PEEQ) in the Al/SiC nanolayered composite at (a) the end of the third cycle and (b) the end of the sixth cycle.

4.4 Comparison with Experiment

This section discusses the comparison of the control model and multilayer model to the experimental measurements of the cyclic nanoindentation response. The models were again compared to the experimental results presented in chapter 3.

The experimental results are shown again in figure 4.12. Figure 4.12(a) shows the measured load-displacement curves of the control specimen. It is evident that there is a drift toward larger displacements starting from the first loading phase. Unloading and reloading largely followed the same path, except at the end of each reloading. Near stabilization was reached after several cycles. Qualitative agreement between experiment and modeling (figure 4.9) for the control specimen is obtained.

Figure 4.12(b) shows the measured indentation response for the Al/SiC multilayers. Again, all prominent features are consistent with the modeling (figure 4.10). Unlike the control case, distinct hysteresis loops now exist, and the open loops progressed toward deeper penetration over the cycles. The inelastic nature of the unload/reload response is evident, and deformation has not reached stabilization at the end of the test. It is concluded that plastic deformation during the cyclic unload/reload process is a distinct feature of the nanolayered metal/ceramic composite.

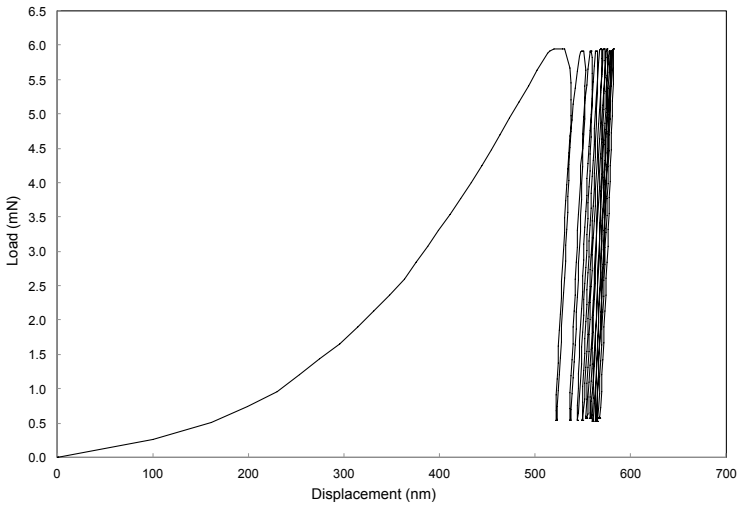

(a)

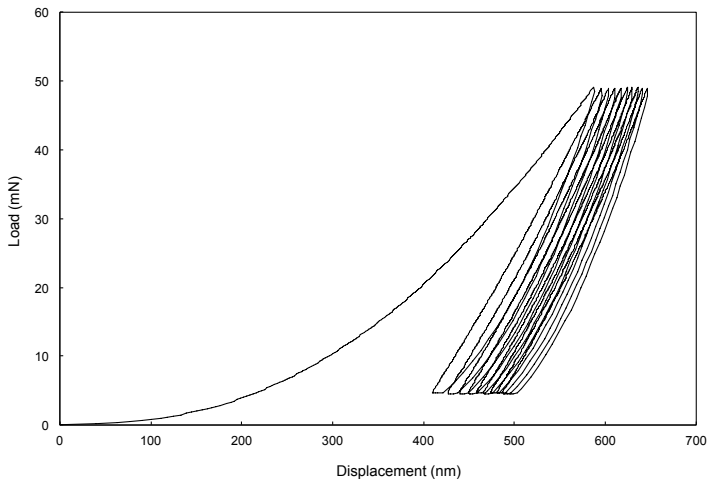

(b)

Figure 4.12: Experimentally measured cyclic nanoindentation load-displacement response of (a) the control specimen (with a thick Al film) and (b) the Al/SiC nanolayered composite.

4.5 Conclusions

With time-dependent viscoplasticity taken into account, the modeling results showed that plastic deformation in the ductile metallic layers continues to occur during the unloading phase of the first cycle, as well as during subsequent reload/unload processes. The cyclic plasticity results in an open load-displacement loop, and the maximum indentation depth continues to increase with each cycle under a constant load amplitude. As in chapter 3, tracking of the deformation history of individual material elements provided insight on how the deformation in the soft metal is constrained by the adjoining hard ceramic layers. Unloading-induced plastic deformation does not occur in the control model. Beyond the first loading cycle, this reference case of a homogeneous Al film shows only very limited inelastic deformation at the end of each reloading phase due to the viscoplastic effect, with the cycling gradually stabilizing into a repetitive elastic response. Nanoindentation experiments under the same type of cyclic loading condition showed good agreement with the modeling, for both the Al/SiC nanolayers and the Al control specimen.

Chapter 5

Conclusions and Suggested Future Work

In this research, numerical finite element analyses was conducted to study the response of a nanolayered composite to cyclic loading. Results from modeling were compared to experimental results. Emphasis was placed on the inelastic deformation experienced by the material during the unloading and reloading processes. Due to the scarcity of experimental and numerical studies on cyclic indentation (even for homogeneous materials), the current work is believed to fill an important void and point to a new direction in materials and mechanics research. Specific salient findings are summarized below.

- Plastic deformation continues to occur in the soft metal layers during unloading, resulting in open load-displacement loop where the maximum indentation depth continues to increase with each consecutive cycle. Experimental results qualitatively agreed with modeling results.
- Tracking the deformation histories of material elements provided insight on how deformation in the soft metal occurs with the constraint of the hard layers.

- Unloading induced plasticity does not occur in the homogenous Al film. However, when the rate-dependent plasticity of the Al is taken into account (compared to the static case), a slight increase in plastic strain is observed at the peak load of subsequent cycles. The observed plasticity will eventually stabilize to an elastic response. This agrees with the experimental results.
- The modeling results raised the issue of possible indentation fatigue damage in the layered composite, which is worthy of further investigations.

The following is suggested future work

- The current model does not yet reach stabilization. It is apparent in the results that the model will eventually stabilize. It would be interesting to see how many more cycles would be necessary to reach stabilization.
- Both models were indented to the same depth. Indenting to different depths would give a better understanding how the composite responds to different peak indentation loads.
- Only one combination of layer thicknesses was tested. Changing the thickness, material parameters and number of the layers will give better insight as to how these properties affect the numerical model.
- Continued experimental work will help validate the numerical models. More systematic experimentation would be helpful in developing a useful numerical model.

References

[1] J. L. Bucaille, S. Stauss, E. Felder, and J. Michler. Determination of plastic properties of metals by instrumented indentation using different sharp indenters. *Acta Materialia*, 51(6):1663 – 1678, 2003.

[2] K. D. Bouzakis, N. Michailidis, and G. Erkens. Thin hard coatings stress–strain curve determination through a fem supported evaluation of nanoindentation test results. *Surface and Coatings Technology*, 142–144(0):102 – 109, 2001.

[3] A. K. Bhattacharya and W. D. Nix. Finite element simulation of indentation experiments. *International Journal of Solids and Structures*, 24(9):881 – 891, 1988.

[4] L. Min, C. Wei-Min, L. Nai-Ganga, and W. Ling-Dong. A numerical study of indentation using indenters of different geometry. *Journal of Materials Research*, 19(1):73–78, 2004.

[5] R. Major, P. Lacki, R. Kustosz, and J.M. Lackner. Modelling of nanoindentation to simulate thin layer behaviour. *Bull. Polish Academy of Sciences: Technical Sciences*, 54(2):189–198, 2006.

[6] X. Chen and J. J. Vlassak. Numerical study on the measurement of thin film mechanical properties by means of nanoindentation. *Journal of Materials Research*, 16:2974 – 2982, October 2001.

[7] P. Montmitonnet, M. L. Edlinger, and E. Felder. Finite element analysis of elastoplastic indentation: Part i—homogeneous media. *Journal of Tribology*, 115(1):10–14, 1993.

[8] D. Ma, K. Xu, and J. He. Numerical simulation for determining the mechanical properties of thin metal films using depth-sensing indentation technique. *Thin Solid Films*, 323(1):183–187, 1998.

[9] A. C. Fischer-Cripps. *Nanoindentation*. Springer, 2002.

[10] W.C. Oliver and G.M. Pharr. An improved technique for determining hardness and elastic modulus using load and displacement sensing indentation experiments. *Journal of Materials Research*, 7(6):1564–1583, June 1992.

[11] P. Jonnard, K. Le Guen, M.-H. Hu, J.-M. André, E. Meltchakov, C. Hecquet, F. Delmotte, and A. Galtayries. Optical, chemical, and depth characterization of al/sic periodic multilayers. *Proc SPIE*, 2009.

[12] D. L. Windt and J. A. Bellotti. Performance, structure, and stability of sic/al multilayer films for extreme ultraviolet applications. *Appl. Opt.*, 48(26):4932–4941, September 2009.

[13] R. C. Cammarata. Mechanical properties of nanocomposite thin films. *Thin Solid Films*, 240(1–2):82 – 87, 1994.

[14] A.T. Alpas, J.D. Embury, D.A. Hardwick, and R.W. Springer. The mechancial-properties of laminated microscale composites of al/al2o3. *Journal of Materials Science*, 25(3):1603–1609, March 1990.

[15] G. Mearini and R. Hoffman. Tensile properties of aluminum/alumina multi-layered thin films. *Journal of Electronic Materials*, 22:623–629, 1993. 10.1007/BF02666408.

[16] T. C. Chou, T. G. Nieh, T. Y. Tsui, G. M. Pharr, and W. C. Oliver. Mechanical properties and microstructures of metal/ceramic microlaminates: Part i. nb/mosi2 systems. *Journal of Materials Research*, 7(10):2765–2773, 1992.

[17] T. C. Chou, T. G. Nieh, S. D. McAdams, G. M. Pharr, and W. C. Oliver. Mechanical-properties and microstructures of metal ceramic microlaminates .2. a mo/al2o3 system. *Journal of Materials Research*, 7(10):2774–2784, October 1992.

[18] C. H. Liu, W. Z. Li, and H. D. Li. Tic/metal nacrous structures and their fracture toughness increase. *Journal of Materials Research*, 11(9):2231–2235, September 1996.

[19] M. Ben Daia, P. Aubert, S. Labdi, C. Sant, F. A. Sadi, Ph. Houdy, and J. L. Bozet. Nanoindentation investigation of ti/tin multilayers films. *Journal of Applied Physics*, 87(11):7753–7757, 2000.

[20] J. H. Lee, W. M. Kim, T. S. Lee, M. K. Chung, B. K. Cheong, and S. G. Kim. Mechanical and adhesion properties of al/aln multilayered thin films. *Surface and Coatings Technology*, 133–134(0):220 – 226, 2000.

[21] A. Lousa, J. Romero, E. Martinez, J. Esteve, F. Montala, and L. Carreras. Multilayered chromium/chromium nitride coatings for use in pressure die-casting. *Surface and Coatings Technology*, 146:268–273, September 2001.

[22] J. Romero, A. Lousa, E. Martinez, and J. Esteve. Nanometric chromium/chromium carbide multilayers for tribological applications. *Surface and Coatings Technology*, 163:392–397, January 2003.

[23] M. A. Phillips, B. M. Clemens, and W. D. Nix. Microstructure and nanoindentation hardness of al/al3sc multilayers. *Acta Materialia*, 51(11):3171–3184, June 2003.

[24] X. Deng, N. Chawla, K. K. Chawla, M. Koopman, and J. P. Chu. Mechanical behavior of multilayered nanoscale metal-ceramic composites. *Advanced Engineering Materials*, 7(12):1099–1108, 2005.

[25] N. Chawla, D. R. P. Singh, Y. L. Shen, G. Tang, and K. K. Chawla. Indentation mechanics and fracture behavior of metal/ceramic nanolaminate composites. *Journal of Materials Science*, 43(13):4383–4390, July 2008.

[26] D. Bhattacharyya, N. A. Mara, P. Dickerson, R. G. Hoagland, and A. Misra. Compressive flow behavior of al-tin multilayers at nanometer scale layer thickness. *Acta Materialia*, 59(10):3804–3816, June 2011.

[27] D. R. P. Singh, N. Chawla, and Y. L. Shen. Focused ion beam (fib) tomography of nanoindentation damage in nanoscale metal/ceramic multilayers. *Materials Characterization*, 61(4):481–488, April 2010.

[28] P. L. Sun, J. P. Chu, T. Y. Lin, Y. L. Shen, and N. Chawla. Characterization of nanoindentation damage in metal/ceramic multilayered films by transmission electron microscopy (tem). *Materials Science and Engineering: A*, 527(12):2985 – 2992, 2010.

[29] F. L. Wen and Y. L. Shen. Plastic deformation in multilayered thin films during indentation unloading: a modeling analysis incorporating viscoplastic response. *Mechanics of Time-Dependent Materials*, 15:277–291, 2011.

[30] G. Tang, Y. L. Shen, D. R. P. Singh, and N. Chawla. Indentation behavior of metal-ceramic multilayers at the nanoscale: Numerical analysis and experimental verification. *Acta Materialia*, 58(6):2033 – 2044, 2010.

[31] G. Tang, Y. L. Shen, and N. Chawla. Plastic deformation during indentation unloading in multilayered materials. *Journal of Applied Physics*, 104(11):116102, 2008.

[32] K. Kozuki, M. Omiya, K. Kishimoto, and H. Inoue. Study of delamination of thin film coating on cyclic nano-indentation test. *Key Engineering Materials*, 353-358:1842–1845, 2007.

[33] W. C. Oliver and G. M. Pharr. Nanoindentation in materials research: Past, present, and future. *MRS Bulletin*, 35(11):897–907, November 2010.

[34] Te-Hua Fang, Win-Jin Chang, Chao-Ming Lin, and Chun-Chin Chang. Cyclic nanoindentation of semiconductor and metal thin films. *International Journal of Modern Physics B*, 23(30):5639–5647, December 2009.

[35] S. G. Pantelakis, P. V. Petroyiannis, K. D. Bouzakis, and I. Mirisidis. Surface hardness increase of 2024 aluminum alloy subjected to cyclic loading. *Theoretical and Applied Fracture Mechanics*, 48(1):68 – 81, 2007.

[36] J Mueller, K Durst, D Amberger, and M Goken. Local investigations of the mechanical properties of ultrafine grained metals by nanoindentations. In *Nanomaterials by Severe Plastic Deformation*, volume 503-504 of *Materials Science Forum*, pages 31–36. Trans Tech Publications LTD, 2006.

[37] F. Q. Yang and A. Saran. Cyclic indentation of an elastic-perfectly plastic material. *Journal of Materials Science*, 41(18):6077–6080, 2006.

[38] Y.-L. Shen, C. B. Blada, J. J. Williams, and N. Chawla. Cyclic indentation behavior of metal-ceramic nanolayered composites. *Materials Science and Engineering A*, Accepted for publication, 2012.

[39] C. B. Blada and Y. L. Shen. Analysis of plastic deformation in metal-ceramic nanolayers during cyclic indentation. *ASME*, submitted for publication, 2012.

[40] D. R. Lide. *Handbook of Chemistry and Physics*. CRC Press, 76 edition, 1995.

[41] J. Bucaille. A new technique to determine the elastoplastic properties of thin metallic films using sharp indenters. *Thin Solid Films*, 447-448:239–245, 2004.

[42] S. Suresh. *Fatigue of Materials*. Cambridge University Press, 2 edition, 1998.

[43] D. R. P. Singh, N. Chawla, G. Tang, and Y. L. Shen. Anomalous viscoplasticity during nanoindentation of al/sic nanolaminated composites. *Materials Science and Engineering A*, 528(13-14):4608–4614, May 2011.